NIR reflectance spectroscopy of hydrated and anhydrous sodium carbonates at different temperatures

S. de Angelis, C. Carli, F. Tosi, P. Beck, O. Brissaud, B. Schmitt, S. Potin, M.C. C de Sanctis, F. Capaccioni, G. Piccioni

De Angelis et al. 2019, Icarus, 317, 388-411

NIR reflectance spectroscopy of hydrated and anhydrous sodium carbonates at different temperatures

S. De Angelis[1], C. Carli[1], F. Tosi[1], P. Beck[2], O. Brissaud[2], B. Schmitt[2], S. Potin[2], M.C. De Sanctis[1], F. Capaccioni[1], G. Piccioni[1]

1 *Istituto di Astrofisica e Planetologia Spaziali, Via del Fosso del Cavaliere, I-00133 Roma, Italy*
2 *Université Grenoble Alpes, CNRS, Institut de Planétologie et d'Astrophysique de Grenoble (IPAG), 38058 Grenoble Cédex 9, France*

Abstract

Recent space-based observations have revealed or suggested the existence of various types of carbonate salts in several Solar System bodies, such as Mars, Ceres, Enceladus, and Europa. Natrite is the main component of the crater Occator's faculae observed in detail by the Dawn spacecraft on the dwarf planet Ceres. Sodium carbonates are thought to form as precipitates in brines, originating in aqueous environments in the subsurface of Ceres and icy bodies. Here we report about near-infrared (0.8-4.2 μm) reflectance spectroscopic investigations on three compounds, namely natrite (anhydrous Na_2CO_3), monohydrated sodium carbonate ($Na_2CO_3 \bullet H_2O$, thermonatrite) and decahydrate sodium carbonate ($Na_2CO_3 \bullet 10H_2O$, natron). Spectral measurements have been carried out in the overall temperature range 93-279 K, representative of planetary surfaces. The analysis of diagnostic spectral signatures shows different temperature-dependent trends for several band parameters, as well as different behavior as a function of the the grain size for a given temperature. While spectra of natrite are characterized by several CO_3 absorptions, broad and strong absorption features due to H_2O dominate the spectra of heavily hydrated natron. The intermediate sample (monohydrated) shows multiple bands due to the overlap of CO_3 and H_2O vibrational modes. Our temperature-dependent laboratory spectra are compared with Dawn-VIR spectra of Ceres and with Galileo-NIMS spectra of Europa.

1. Introduction

Sodium carbonate minerals are rarely seen on the surfaces of Solar System bodies other than the Earth, both in the anhydrous form and in hydrated forms. Remote sensing observations returned by planetary space missions have confidently identified various types of carbonate compounds in different hydration states on Mars and on the dwarf planet Ceres, while their existence has been ascertained in Saturn's satellite Enceladus and suggested in Jupiter's satellite Europa.

Occurrence of Na-carbonates on Earth.
On Earth, anhydrous and hydrated sodium carbonates appear in different environments. Natrite (Na_2CO_3) is not widespread and typically occurs in localized volcanic areas, especially in pegmatites from alkaline massifs (Russia) (Khomyakov, 1983) or in xenoliths from intrusive alkaline complexes (Canada) (Anthony et al., 2003), and rarely it also occurs in carbonatites (Jones et al., 2013). The two most common hydrated phases, thermonatrite ($Na_2CO_3 \bullet 1H_2O$) and natron ($Na_2CO_3 \bullet 10H_2O$), are evaporite minerals typically found in saline lacustrine environments (Jones & Deocampo, 2003). In particular, these minerals are frequently associated with sodium-rich waters produced in geologic settings where calc-alkaline volcanic activity was predominant, and Na^+ ions are often the most common species

in solution (Jones & Deocampo, 2003). In the chemical evolution path of brine due to evaporation, typically Na-carbonates are the last species to precipitate, following the sequence: Ca-Mg carbonates → gypsum → Mg-sulfates → Na-sulfates → Na-carbonates. Rarely thermonatrite and natron are also found as high temperature fumarole volcanic products (Russo, 2006).

Ceres.

Spectroscopic observations by the Visible and InfraRed mapping spectrometer (VIR) onboard the NASA Dawn mission indicate that the bright material units (*faculae*) seen in the floor of the 92-km crater Occator on Ceres are mainly composed of natrite (Na_2CO_3) mixed with phyllosilicates, ammonium chloride and a dark, spectrally featureless absorbing material (De Sanctis, et al., 2016; Raponi et al., 2018). Many other occurences of Na-carbonates have been identified on Ceres (Carozzo et al., 2018; De Sanctis et al., 2017), mostly in anhydrous form. The main evidence for natrite in the Ceres spectra of Occator's faculae comes from the shape and central wavelengths of the of CO_3^{2-} absorption bands at approximately 3.3-3.5 and 3.95-4.0 μm (Hunt & Salisbury, 1971) together with its contribution in increasing the reflectance level with respect to the average spectrum of Ceres (De Sanctis, et al., 2016). Occator's faculae spectra show strong carbonate bands, with a clear shift of the band center longward of 3.98 micron, which is indicative of sodium carbonate. The estimated amount of sodium carbonate in Cerealia Facula, i.e. the brightest spot found in crater Occator and one of the brightest spots across Ceres, is up to 70-80 vol%, making it the largest carbonate concentration found on an extraterrestrial body (De Sanctis et al., 2016; Raponi et al., 2018).

Its co-occurrence with ammonium salts near impact craters on Ceres has been interpreted as due to liquid brines upwelling from depth and crystallization on the surface (Zolotov, 2017). The formation mechanisms and stability fields of natrite and other chemical species have been recently investigated both in terms of laboratory experiments and modeling. Based on laboratory studies of freezing liquid brines containing Na^+ – $(NH_4)^+$ – Cl^- – $(CO_3)^{2-}$ ions, Vu et al. (2017) showed that mainly preferential precipitation of Na-carbonates occurs due to the lowest aqueous solubility at cryogenic temperatures, confirming the scenario in which natrite crystallized on the surface of Ceres from liquid brines ascending from below. Zolotov (2017) used a chemistry model to investigate the formation of compounds starting from water solutions containing H-C-N-O-Na-Cl ions. Natron and nahcolite ($NaHCO_3$) precipitate/crystallize as starting species in liquid brines reaching the surface of Ceres, and subsequent dehydration, due to instability at vacuum conditions, results in deposition of Na_2CO_3.

The laboratory detailed spectral analyses of natrite and natron at cryogenic temperatures will be of interest for the analyses and interpretation of Dawn data, as well as for data from future missions to Ceres.

Europa.

Sodium compounds have been suggested to exist on the surface of Jupiter's icy Galilean moon Europa, both in the form of carbonates and sulfates, in various hydration states and mixed with water ice (Carlson et al., 2009). In particular, natron is among the best candidates to explain spectra of visually dark, non-icy terrains on Europa (McCord et al., 1998a) as revealed by the Near Infrared Mapping Spectrometer (NIMS) onboard the NASA Galileo spacecraft (Carlson et al., 1992). Spectra of non-icy terrains as measured by Galileo-NIMS display broadened and distorted water ice absorption features in the 1-3 μm region, combined with the lack of metal-OH signatures. This has been interpreted as evidence for a high hydration state, i.e. a high number of H_2O molecules bonded in the mineral structure in different crystal sites, pointing to the presence of heavily hydrated sodium carbonates (e.g., natron), likely

intermixed with Mg-sulfates, rather than clays and phyllosilicates (McCord et al., 1998b). Although a specific salt mineral perfectly matching the spectral profiles of Europa in non-icy regions has not been yet unanimously identified, natron has been used as a plausible spectral endmember in mixtures to model the measured NIMS spectra, together with hydrated Mg-sulfates such as bloedite, mirabilite, hexahydrite, and epsomite (McCord et al., 1999; McCord et al., 2010). Previous laboratory studies (see for example Dalton et al., 2005; De Angelis et al., 2017) have investigated the temperature-dependent behavior of magnesium sulfates as analogues for the Europa spectra modeling. Further laboratory work on hydrated Na-carbonates at cryogenic temperatures will be helpful in the comprehension of data from future missions to Europa and Jovian icy moons (ESA/JUICE and NASA/Europa Clipper).

Enceladus.
Sodium salts have been reported to occur in Saturn's E-ring, which originates from the jets emanating from the southern polar region of its icy moon Enceladus. In particular Na_2CO_3, NaCl and $NaHCO_3$ were detected *in situ* by the Cosmic Dust Analyser onboard the Cassini spacecraft (Postberg et al., 2009, 2011). The sodium salts observed by means of mass spectrometry within both Saturn's E-ring and the plumes of Enceladus are believed to originate from a liquid ocean located some tens of km beneath the surface (Postberg et al., 2009, 2011).

Mars.
Carbonates with different compositions have been detected on Mars by means of remote sensing techniques, both in the atmospheric dust and on the surface, as well as by *in situ* instruments onboard landers and rovers (Niles et al., 2013). Nevertheless, the observations are so far in agreement with the presence of Ca-Mg-Fe carbonates, while Na-carbonates have not yet been detected. For example, carbonates in martian dust have been observed by means of thermal infrared measurements obtained by the Thermal Emission Spectrometer (TES) onboard Mars Global Surveyor (Bandfield et al., 2003). Several spectroscopic evidences obtained from orbit attest the presence of carbonates on the surface (Ehlmann et al., 2008; Ehlmann & Edwards, 2014; Wray et al., 2016), while MER rovers (Morris et al., 2010) and the Phoenix lander (Boynton et al., 2009) also evidenced their occurrence in several sites.

So far sodium carbonates have been missing both in remote sensing observations and in landers/rovers analyses at Mars, although their presence is predicted by models. According to some authors Na-carbonates, which are highly soluble, should be present in the upper layers of a model evaporitic sedimentation stratigraphy (Catling, 1999), while Fe/Mg-carbonates are expected to be deeply buried. In this case Na-carbonates would be completely hidden by the oxidized surface layer. Other authors (Grotzinger & Milliken, 2012) point out that the global low-pH (acidic) conditions of ancient Martian aqueous environments prevented the formation of Na-carbonates on a global scale. According to McLennan (2012) sedimentary secondary minerals tend to be Fe- and Mg-rich and Na- and K- poor, reflecting differences in crustal composition between Earth and Mars as well as differences in the aqueous environment of alteration (more acidic).
In-situ data from forthcoming rover missions (ESA/ExoMars 2020, NASA/Mars 2020) will provide additional information about mineralogy at small scales, and data interpretation will be aided by detailed laboratory studies of sodium (and not only) carbonates at low temperatures.

Laboratory studies.

Several laboratory studies exist up to now that investigated sodium carbonates in detail by means of visible-near infrared (NIR) spectroscopy and at various P-T conditions. Bujis & Schutte (1961a,b) measured mid-infrared transmission spectra of anhydrous sodium carbonate and various forms of its hydrates, at room temperature. Mid-infrared (Mid-IR) spectra of natrite were acquired in the 5-50-μm range at 300K and 80K by Brooker & Bates (1971). Meekes et al. (1986) published reflection spectra of natrite at various temperatures in the far infrared (Far-IR, 25 μm – 0.1 mm), and also Harris & Salje (1992) investigated anhydrous sodium carbonate by means of transmission spectroscopy in the mid-IR (5-25-μm) at various temperatures. McCord et al. (2001) measured Near-IR spectra (1-2.7 μm) of natron, together with mirabilite and epsomite, under vacuum conditions at ambient and cryogenic temperatures in the range 100-300K, in order to study the stability field of these minerals. Crowley (1991) and Harner & Gilmore (2015) acquired spectra of natron, among many other evaporitic playa minerals, in the 0.35-2.5-μm range at room temperature. Drake (1995) and Harner & Gilmore (2014) published room temperature reflectance spectra of thermonatrite in the 0.35-2.5-μm range.

Several studies report on the phase transitions underwent by Na_2CO_3 because of temperature variations. Natrite presents four phases: α, β, γ, δ in the temperature range <170-1000K. In the 170-605K temperature range, natrite is in the form γ (incommensurate, space group *C2/m*) with cell parameters a=8.920 Å, b=5.245 Å and c=6.050 Å (Harris & Salje, 1992; Arakcheeva & Chapuis, 2005). For temperatures below 130-170K, natrite undergoes a fourth phase transition, to δ-phase named "lock-in", with cell parameters a=8.898 Å, b=5.237 Å and c=5.996 Å (Meekes et al., 1986; Arakcheeva & Chapuis, 2005). In the δ-phase below 130K the sodium carbonate assumes a commensurate structure. As the temperature decreases, a gradual strengthening of C–Na interactions occurs, with shortening of C–Na interatomic distances. The number of C–Na bonds (Na^+ ions surrounding C atoms) increases as T decreases. These changes produce modifications in the O atomic positions, and result in increasing of C–O distances, and tilting and distortion of CO_3 units (Arakcheeva & Chapuis, 2005). Moreover, order-to-disorder changes are related to phase transitions, involving changes in the structure of lattice bands (Brooker & Bates, 1971). Meekes et al. (1986) in their IR and Raman study observe a change with temperature in peak intensity relative to ν_1 frequency mode (1080 cm^{-1}). In general they report the appearance of new sharp absorption lines in mid-IR and Raman spectra acquired below 130 K, instead of broad bands occurring at higher temperatures. Analogously Harris & Salje (1992) report the appearance of two weak absorption bands in their IR spectra at low temperatures. They measured IR spectra in the 5-25-μm range and in the 45-800K temperature range, finding that new absorption features appeared in the 14 μm region (ν_4 fundamental vibration) in <130K spectra: the room-temperature band corresponding to ν_4 consists of two peaks, while below 130K it is composed of seven separate peaks. In our measurements we do not probe the mid-IR range, so we are not directly sensitive to the fundamental carbonate vibrations, but only to their overtones and combinations. Nevertheless, the temperature-dependent spectral changes that we observe in the VNIR are undoubtedly related to the change in the mineral structure. Here we probe the overtone at 2.12-2.16 μm ($\nu_1+2\nu_3+\nu_4$ or $3\nu_1+2\nu_4$), so we expect some changes could be seen below 130K in this feature, although probably requiring very high spectral resolution.

In all these works cryogenic spectra of natrite are only described in the range above 5 μm and in transmission mode (Brooker & Bates, 1971; Harris & Salje, 1992). Thus cryogenic

reflectance spectra of natrite in the <5 μm spectral range seem to be lacking in the literature. Concerning natron, cryogenic spectra are only described at 100K (McCord et al., 2001) and in the 1-2.7 μm range: so cryogenic reflectance spectra of natron are lacking in the 2.7-5 μm range. Finally no cryogenic spectra of thermonatrite seem to be present in the literature.
Moreover literature transmission studies typically focused on samples in thin films. Reflectance studies instead used single grain size ranges (d<125 μm (Harner & Gilmore, 2015) or 355-500 μm (McCord et al., 2001)) or generic powders. A systematic work is thus missing dedicated to a comparative study of different grain sizes.

Our work.
In this laboratory work we present the results of near infrared reflectance spectroscopy measurements obtained for three sodium carbonates, two hydrated and one anhydrous, namely natrite (Na_2CO_3), thermonatrite ($Na_2CO_3 \bullet H_2O$), and natron ($Na_2CO_3 \bullet 10H_2O$). Reflectance spectra were acquired for these samples, in the 0.8-4.2-μm range, in three different grain sizes, and at several temperatures in the overall range 93-279 K.
While previous work mainly focused on a particular type of sample at a fixed temperature, here we describe a systematic comparative spectral study on sodium carbonate in its anhydrous form and in its two natural hydrated stable forms.
Our study is based on the analyses of spectral data for numerous temperatures (10-11 steps for each ramp) in the above-mentioned range; other studies concerning low-temperature measurements described spectra acquired at few selected temperatures.
Here we also present a systematic study dealing with different grain sizes and comparing their spectral effects.

In Section 2 we describe the experimental setup that we used at the Institut de Planétologie et d'Astrophysique de Grenoble (IPAG). In Section 3 and 4 we present the spectral analysis and results, followed by a discussion in terms of their relevance for Ceres and Europa.

2. Methods.

2.1 Experimental setup

Our measurements were carried out in November 2016 with the SHINE Spectro-Gonio Radiometer facility (Brissaud et al, 2004) at the Institut de Planétologie et d'Astrophysique de Grenoble (IPAG). The instrument is a bidirectional VIS-NIR reflectance spectrometer, which we operated in the overall 0.8–4.2-μm spectral interval by means of two detectors: a silicon photodiode in the 0.5–1.0 μm range and an InSb IR detector in the 1.0–4.2 μm range. The anhydrous sample was acquired in the range 1-4.2 μm, in order to fully measure the carbonate band at 4 μm. Conversely, the two hydrated samples were acquired in the range 0.8-4.0 μm. This choice was motivated by the fact that the 3-4 μm region is expected to be dominated by water absorption, and by the time required to measure the full range up to 4.2 μm.
The sample is illuminated with monochromatic light. Spectralon and Infragold (Labsphere ©) were used as standard reference targets, measured at room temperature and radiometrically characterized in terms of BRDF (Bonnefoy 2001). All spectra were acquired with an illumination angle i = 0° and an emission angle e = 15°. We used the following spectral sampling: (i) natrite, Δλ=20 nm in the 0.8-4.2 μm range; (ii) thermonatrite and natron, Δλ=20 nm in the 0.4-1.2 μm range, Δλ=10 nm in the 1.2-3 μm range, Δλ=20 nm in the 3-4.2 μm

range. The average spectral resolution was: 10 nm for λ=0.8–1.6 μm, 19 nm for λ=1.6–3.0 μm, and 39 nm for λ=3.0– 4.2 μm.

The CarboN-IR environmental chamber coupled with the spectro-gonio-radiometer (Grisolle 2013; Grisolle et al., 2014; Beck et al., 2015) was used to perform measurements. The chamber consists of a large closed isothermal copper cell (8-cm diameter) placed within a stainless steel chamber. The sample is placed within the inner closed cell. A helium cryocooler is used to cool down the cell and the optical access is enabled by a sapphire window viewport. This setup allows the acquisition of reflectance spectra at temperatures down to 50 K. A few mbar of dry air were purged into the cell with the aim of ensuring efficient thermal coupling of the sample and avoiding dehydration. The temperature of the cell is monitored during the measurement runs, and the associated error on the effective sample temperature is of the order of 1 K.

2.2 Samples

We analyzed three sodium carbonate compounds: natrite (anhydrous, Na_2CO_3), thermonatrite ($Na_2CO_3 \bullet H_2O$), and natron ($Na_2CO_3 \bullet 10H_2O$). These samples are available on the market, supplied by Sigma Aldrich and characterized by a >99% purity level. All materials were ground, sieved and sorted at three different grain sizes: 36-50 μm, 75-100 μm, and 125-150 μm. The choice of these grain size ranges is motivated by measuring fine, medium and coarse particles, avoiding at the same time any overlap in particle dimensions among these three classes. These grain sizes fall in the range of particle dimensions that constitute typical planetary regoliths (20 μm < d < 20 mm (Gundlach & Blum, 2013)). In particular for Ceres regolith the mean expected grain size is about 100 μm. According to Hapke modeling (De Sanctis et al., 2015) grain sizes in the range 2-190 μm are expected for minerals and 300 μm for water ice. Concerning Europa surface particles sizes in the range between d<50 μm and a few hundreds of micrometers are inferred from NIR observations (McCord et al., 1999).

2.3 Spectra acquisitions and data reduction

Reflectance spectra were acquired at different temperatures for each grain size (Figs. 1-3), in the range 93-279 K. The first spectrum was acquired at room temperature (279 K), whereas all other measurements were recorded starting from the lowest temperature (T_0 = 93 K) and acquiring consecutive spectra at increasing temperature values, up to 279 K again. Measurements have been performed at steps of 10-15 K in the low temperature range, and at steps of 20-25 K in the high temperature range, for a total of 10-11 steps on average for each grain size.

Different spectral parameters were computed starting from the measured spectra: band area, band depth, band width, and band position for each of the absorptions visible in the spectra. The reflectance value has also been evaluated for the three samples, at 279 and 93 K, as a function of the water content (see Section 4: Discussion).

All of the spectral indices have been computed after removing the spectral continuum: a straight line has been drawn between the edges for each band, by intersecting the visually identified maxima on both sides of the band (Fig. 4), and then has been removed by dividing the spectrum by this line. For each grain size and a given absorption band, shoulder positions used for continuum removal were the same for all spectra (all temperatures). We applied a second-order polynomial fit around the band minimum (after resampling) in order to compute the band position value (minimum of the fit). Following Clark & Roush (1984), we determined the band depth as: $D = (R_C - R_B)/R_C$, where R_B and R_C are the reflectance factor of the band at its minimum and the level of the spectral continuum at the position of the band

minimum, respectively. The width has been computed by intersecting the continuum-removed band with a horizontal line passing through half depth. Finally the band area has been computed between the continuum maxima as the total area between the continuum line and the absorption band. For those absorption bands showing multiple minima, the spectral continuum is computed between the two shoulders of the band, and the position of each single minimum is fitted with a second-order polynomial. The band area and band width are also computed only for the entire band and not for every single relative minima, for which it is not unambiguous to select the shoulders. The features near 1 μm are likely instrumental artifacts and thus they have not been analyzed. All retrieved spectral parameters and input shoulder positions for continuum removal are listed in tables in the Supplementary Material.

3. Results

3.1 Spectral measurements

In Fig. 1-3 we summarize respectively the measured spectra of natrite (Fig. 1), thermonatrite (Fig. 2), and natron (Fig. 3). For each mineral, the spectra corresponding to the measured temperatures in the range 93-279 K are shown separately for the three analyzed grain sizes: the fine one (36-50 μm) in the top panel, the medium one (75-100 μm) in the central panel, and the coarse one (125-150 μm) in the bottom panel. In each plot, the top spectrum (dashed line) is the first spectrum acquired at room temperature (279 K), then all the spectra are shown in order of increasing temperature from bottom to top: from 93 (always the second acquired spectra) back to 279 K, from bottom to top. The spectra are offset by 0.1 in reflectance for clarity.

3.1.1 Anhydrous Sodium carbonate (natrite)

The spectra of anhydrous sodium carbonate (Fig. 1) are characterized by combinations and overtones of CO_3^{2-} absorption bands located near 2.2, 2.35 and 2.55 μm (Gaffey, 1986, Clark et al., 1990), whose fundamental vibrational transitions are located in the 7-14-μm region. A very weak feature appearing near 1.75 μm could also be due to CO_3^{2-} absorptions (Gaffey, 1986), although we did not analyze it. Some H_2O/OH^- could be responsible for the faint absorption at 1.55 μm and for the band at 2.0 μm, although the latter overlaps with a CO_3^{2-} absorption (Gaffey, 1986, Clark et al., 1990). The 3-4 μm spectral region is characterized by the two strong CO_3^{2-} absorptions appearing around 3.4 and 3.9 μm, which are diagnostic of anhydrous carbonates (Buijs & Schutte, 1961a; Hunt & Salisbury, 1971). In particular, the 3.4 μm feature (2900 cm^{-1}) is assigned to the overtone $2\nu_3$ of the fundamental vibration ν_3 occurring at 6.9 μm (1451 cm^{-1}), while the 4 μm feature (2500 cm^{-1}) is assigned to a combination $\nu_1+\nu_3$ of the fundamental vibrations ν_1 at 9 μm (1079 cm^{-1}) and ν_3 (Buijs & Schutte, 1961a; Nuevo et al., 2014). Both features are characterized by two separate minima that appear as doublets at 3.4-3.5 and 3.8-4.0 μm, whose relative strength varies as a function of temperature. In the 3 μm region the broad absorption band is likely due to absorption by ambient water molecules adsorbed on the sample (Farmer, 1974). A very faint and narrow feature appears near 2.65 μm in almost all spectra, although it remains unassigned. It could be in principle due to water vapor present along the external optical path. A narrow absorption also appears at 3.1 μm at cryogenic temperatures, putatively due to some water condensation (see Discussion Section below). It must be noted that the preparation and manipulation in the laboratory of the anhydrous sample result in moderate hydration of natrite, which in fact is unavoidable due to the hygroscopic nature of the compound. The overall reflectance level at

the continuum background (near 1 μm) does not show any clear correlation with temperature, for the anhydrous as well as for the hydrated forms. Fluctuations in the reflectance level of the order of <10% occur as the temperature change. Instead a correlation is seen with the hydration state; we examine this aspect in section 4.4.

3.1.2 Sodium carbonate monohydrated (thermonatrite)

Spectra of thermonatrite are shown in Fig. 2. These spectra are characterized both by an increased complexity and by an overall notable reduction of the reflectance longward of 1.5 μm, because of the presence of water molecules bonded within the crystal structure of the mineral. Several hydration bands due to vibrational transitions in H_2O molecules appears in several locations, most of which combine and overlap with the absorption features due to CO_3^{2-} ions. In spectra acquired at room temperature, the main recognizable absorption bands occur at 1.25, 1.6 μm, 1.8 μm, 2.0 μm, 2.5 μm, 2,65 and 3.0 μm. The bands at 2.0 and 2.5 μm display a composite structure that becomes more complex as the temperature decreases. At room temperature, the 2.35-μm CO_3^{2-} absorption appears as a shoulder within the 2.55 μm carbonate band, while at the lowest temperatures the 2.5-μm band splits in three separate narrow minima. In the 3-4 μm region, the intense water absorption generally gives a very low reflectance level while the carbonate bands are greatly attenuated; the broad 3-μm H_2O band becomes more defined at low temperatures, while the reflection peak near 3.8 μm becomes more evident and shifts towards shorter wavelengths. At room temperature, strong absorption by water produces saturation in the 3-μm region. This saturation is stronger in the spectra of the sample with grain size 75-100 μm and even more evident in spectra of the samples at 125-150 μm, where the 3-μm band is almost flat. On the contrary, the 3-μm band in 36-50 μm spectra is evident also in measurements acquired at room temperature. Furthermore, in the finest grain size a change in the spectral slope at 3.5 μm is likely the result of the nearby 3.4 μm absorption due to CO_3^{2-}.

3.1.3 Sodium carbonate decahydrate (natron)

Figure 3 shows the spectra of sodium carbonate decahydrate, or natron. The high water content is responsible for most of the absorption features. The bands occurring at 1.0, 1.25, 1.5, 2.0 and 3.0 μm are due to combinations and overtones of the water molecule (Farmer, 1974; Clark et al., 1990). The CO_3^{2-} transitions are responsible for an absorption close to 2.45 μm, for an absorption near 1.75-1.8 μm, although comprised within the broad 1.5-μm band, for the change in the spectral slope near 3.5 μm and for the drop in reflectance towards 4 μm. With respect to the thermonatrite spectra, the higher hydration state of natron results in H_2O bands at 1.5 and 2 μm being very strong and broad and characterized by a less complex fine structure, due to the overlap of various bands corresponding to as many transition modes.

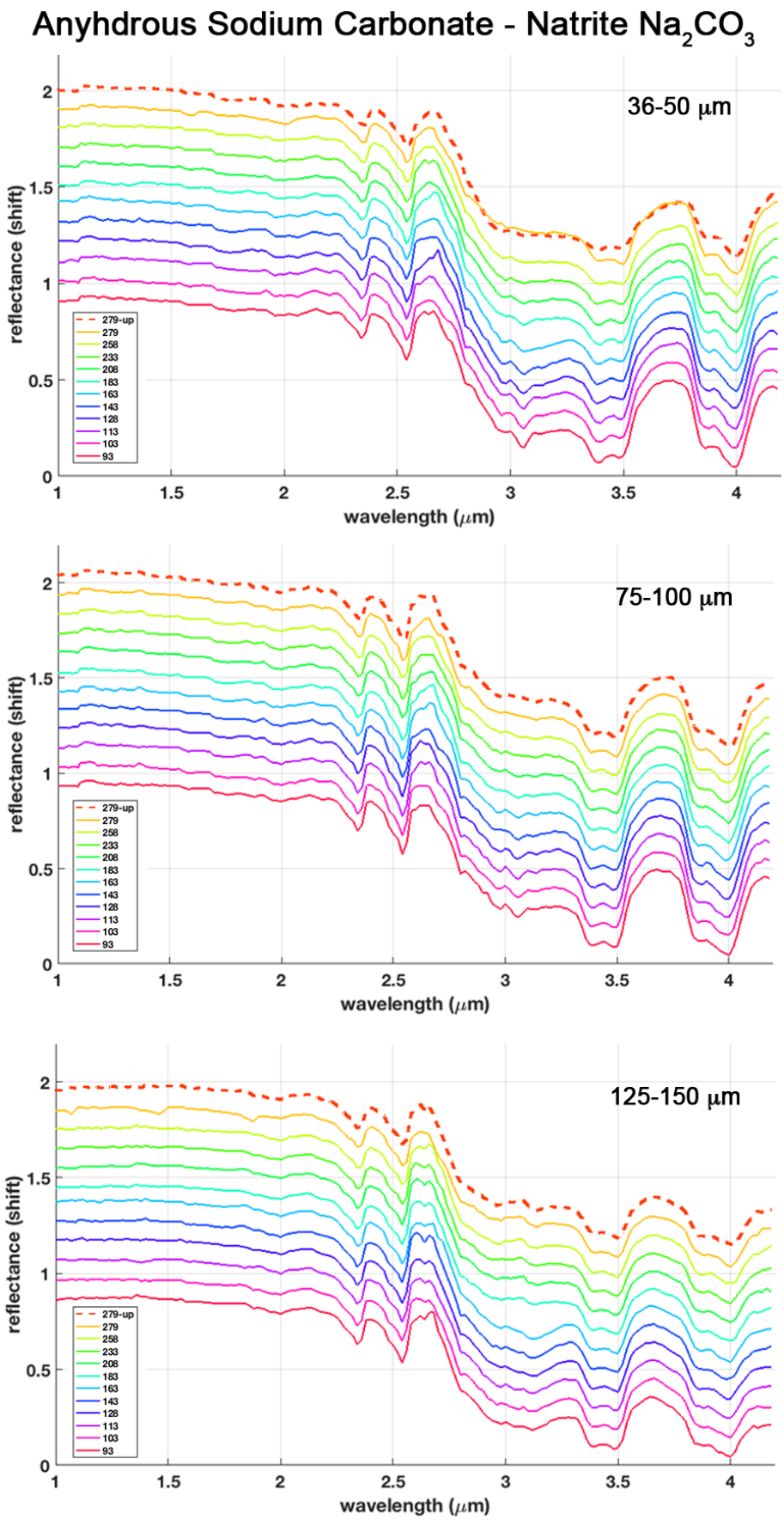

Figure 1. Spectra of anhydrous sodium carbonate (Na_2CO_3) acquired at different temperatures in the range 93-279 K. Measurements at 279 K have been acquired both at the beginning and at the end of the sequence. An arbitrary offset of 0.1 in reflectance is applied to all spectra for clarity. The bottommost spectrum corresponds to the true reflectance value, ≈0.9 at 1 μm.

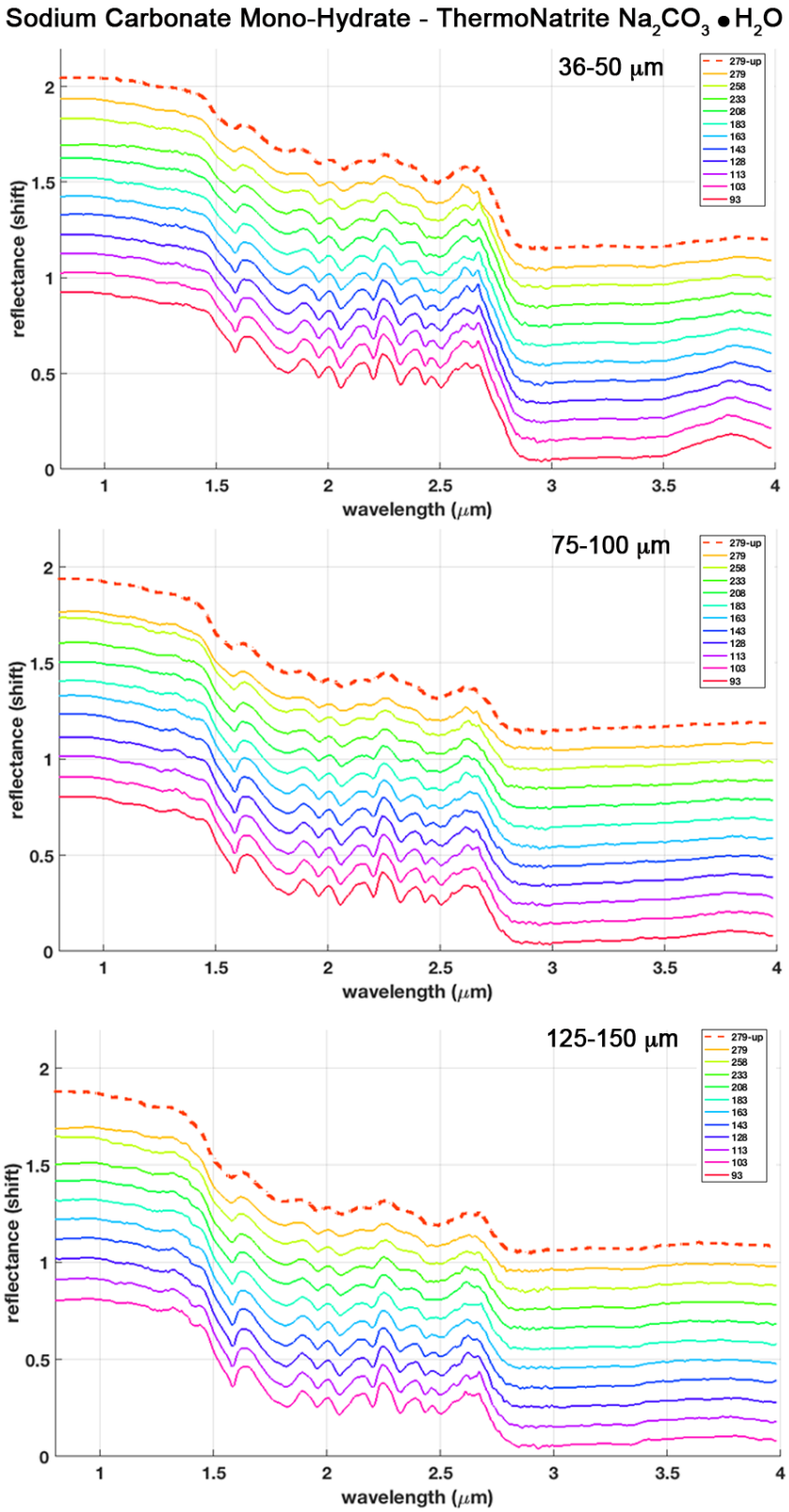

Figure 2. Spectra of monohydrated sodium carbonate ($Na_2CO_3 \bullet H_2O$) acquired at different temperatures in the range 93-279 K. Measurements at 279 K have been acquired both at the beginning and at the end of the sequence. An arbitrary offset of 0.1 in reflectance is applied to all spectra for clarity. For the 125-150 μm grain size the T=113 K spectrum has not been measured. The bottommost spectrum corresponds to the true reflectance value, ≈0.9 at 1 μm.

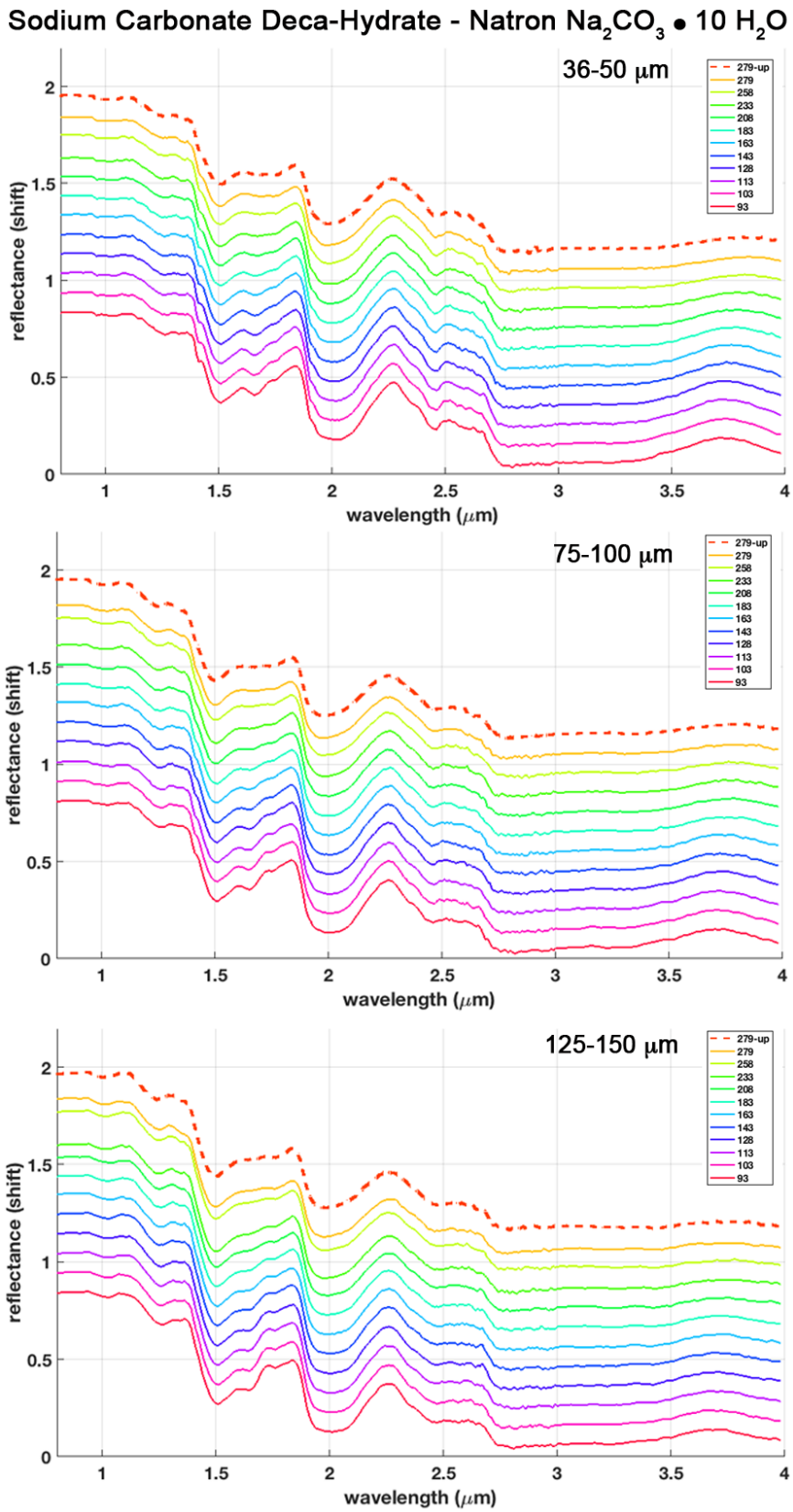

Figure 3. Spectra of decahydrate sodium carbonate (Na_2CO_3 • 10 H_2O) acquired at different temperatures in the range 93-279 K. Measurements at 279 K have been acquired both at the beginning and at the end of the sequence. An arbitrary offset of 0.1 in reflectance is applied to all spectra for clarity. The bottommost spectrum corresponds to the true reflectance value, ≈0.8 at 1 μm.

3.2 Spectral analysis

Spectral indices have been analyzed for each sample grain size and for all the resolved absorption bands. The analyzed features for the three compounds are indicated by the arrows in Fig. 4 and listed in Table 1. For each absorption band, the position, depth, area and width have been computed following the procedure described in Section 2.3. Linear fits have been computed for each spectral index as a function of temperature. In the next sections we describe the results of the spectral analyses. Taking into account the spectral sampling and the resolution of the instrument, here we only report trends for those band positions showing substantial shifts.

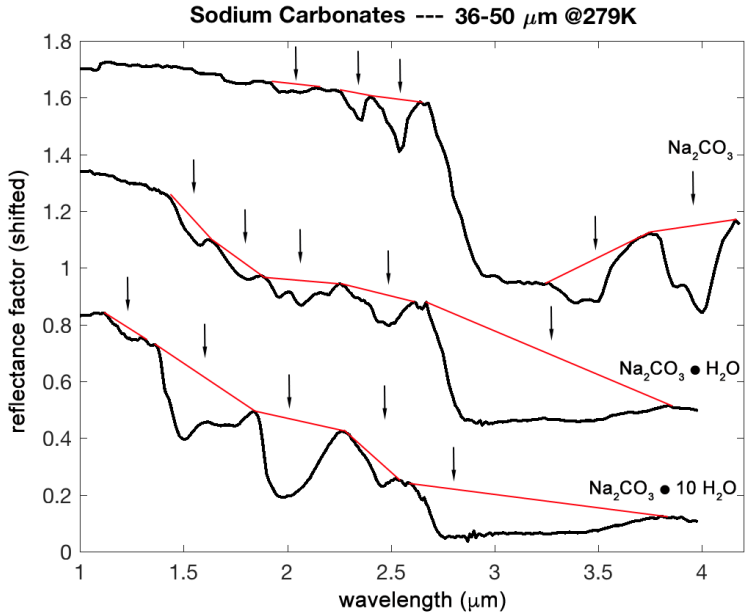

Figure 4. The three analyzed compounds, at 279 K (up), 36-50-μm. The arrows indicate the analyzed bands. See Table 1. The red lines indicate the continuum applied (removed by division). The spectra of Na_2CO_3 and Na_2CO_3•H_2O are respectively offset by 0.8 and 0.4 for clarity.

Compounds	***Bands (μm)***	***Analyses***	***Process***	***Intensity***
Na_2CO_3	1.55		OH/H_2O	vw
	1.75		CO_3	w
	2.0	X	H_2O+ CO_3	w
	2.2		CO_3	w
	2.34	X	CO_3	m
	2.54	X	CO_3	m
	2.65		H_2O (vapor)	vw
	3.0		Adsorbed H_2O	s
	3.40 (I), 3.49 (II)	X	CO_3	s
	3.88 (I), 3.99 (II)	X	CO_3	vs
Na_2CO_3•H_2O	1.25		H_2O	vw
	1.57	X	H_2O	m
	1.78	X	H_2O	m
	1.96 (I), 2.06 (II), 2.20 (III)	X	H_2O+ CO_3	m
	2.32 (I), 2.44 (II), 2.50 (III)	X	CO_3 (+ H_2O)	w/m
	2.65		H_2O (vapor)	vw
	2.9	X	H_2O (+CO_3)	vs
Na_2CO_3•10H_2O	1.0		H_2O	w

	1.23	X	H_2O	w
	1.50 (I), 1.64 (II)	X	H_2O	s/m
	1.75		CO_3	w
	1.99	X	H_2O (+ CO_3)	s
	2.45	X	CO_3	m
	2.8	X	H_2O (+CO_3)	vs

Table 1. List of the analyzed bands for the three compounds, indicated by X. Multiple minima within each analyzed band are denoted by roman numerals and their spectral position presented in the text. Intensity labels, referred to the continuum reflectance level, are: vw = very weak (B_D<5%), w = weak (B_D<10%), m = medium (B_D<30%), s = strong (B_D<50%), vs = very strong (B_D>50%).

3.3 Anhydrous sodium carbonate

3.3.1 2.0-μm band

The band parameters of the 2.0-μm feature (position, depth, area, width) are shown in Fig. 5A. This feature likely results from the combination of H_2O and CO_3^{2-} absorptions. The band depth and band area tend to decrease with increasing temperature values, assuming slightly higher values at lower temperatures, although our measurements display large fluctuations. The maximum depth is assumed by the intermediate grain size (75-100 μm). The band position and band width do not show any clear correlation with temperature. The band position moves to longer wavelengths (2.01-2.02 μm) for the smaller grain size (36-50 μm) compared to the two larger grain sizes (1.98-1.99 μm). Here we must stress that this feature (and all other relative to natrite) display shifts in position that are theoretically below the instrument spectral resolution, although comparable with the spectral sampling. At the same time, we can state that, because we used a consistent method all along our data analysis, we are able to detect relative shifts of positions with a better accuracy, of the order of a few nm.

3.3.2 2.34-μm band

Spectral indices computed for the 2.35 μm CO_3^{2-} absorption feature are shown in Fig. 5B. The band position slightly shifts towards shorter wavelengths as the temperature decreases. The band depth and band area clearly increase almost linearly as the temperature drops down. The band width does not show a clear temperature-dependent behavior, although it appears to be increasing only for the smallest grain size. Both depth and area have maximum values for the intermediate grain size (75-100 μm), whereas they show minimum values for the coarse grain size (125-150 μm).

3.3.3 2.54-μm band

In Fig. 5C we show the 2.55-μm CO_3^{2-} band parameters. Again, the band position very slightly shifts towards shorter wavelengths (2.544-2.540 μm) as the temperature decreases (below spectral resolution), whereas the depth and area have higher values at lower temperatures. The bandwidth is approximately constant. It should be noted that the instrument spectral resolution is 19 nm longward of 2 μm. Again, maximum values of depth and area are found for the intermediate grain size, whereas minimum values occur for the coarse grain size.

3.3.4 3.40-3.49 μm band

The 3.4-μm band, which shows up only in the anhydrous sodium carbonate sample, is characterized by a doublet, with two separate minima occurring near 3.40 μm (I) and 3.49 μm

(II). The band parameters are shown in Fig. 6A, respectively. The position of band I appears to be independent of temperature (Fig. 6A), while the position of band II shows some slight shift towards shorter wavelengths as the temperature decreases (Fig. 6A). Both features display band depth increasing with decreasing temperature; for the 36-50-μm grain size the depth shows an increase of about 25-30%. The area and width are the same for band I and II, having been computed considering the same short wavelength (3.3 μm) and long wavelength (3.7 μm) shoulders of the whole carbonate feature. The area shows an almost linear increase as the temperature decreases, especially for the 36-50 and 75-100-μm grain sizes. In the fine (36-50 μm) and coarse-grained sample (125-150 μm) there is some change occurring at ~160 K. This may be an indirect variation, triggered by the change in strength and shape of the 3 μm band above 163 K: it increases the continuum level at 3.3 μm resulting in an increase of depth and area of the nearby 3.4-3.49 μm bands. The band clearly becomes narrower (decreasing width) towards cryogenic temperatures.

3.3.5 3.88-3.99 μm band

The 4-μm carbonate band, as well as the 3.4-μm band, shows up only in the anhydrous compound, as there is no saturated 3.0-μm water band. Spectral indices are shown in Fig. 6B. Also this band is characterized by a doublet, with two minima occurring around 3.88 and 3.99 μm. The position of both minima shifts towards the shorter wavelengths as the temperature decreases to cryogenic values, while the band depth increases linearly, by 20-30%, especially for the 36-50-μm and 75-100-μm grain sizes. Conversely, this band is more influenced by water absorption in the coarse 125-150-μm grain size, and its variation is not equally clear, although a slight increase seems to occur. A similar behavior is found in the band area, which linearly increases with decreasing temperature, notably for the 36-50 and 75-100-μm grain sizes. The width does not show an unambiguous temperature dependence for all the three grain sizes: it shows an increase towards low temperatures for the 36-50 and 75-100-μm grain sizes, and a decrease for the coarse grain size, likely due to the greater influence of water absorption. The 3.4 and 4 μm carbonate bands both have maximum depth and area values for the intermediate grain size, and minimum values in correspondence of coarse grain size.

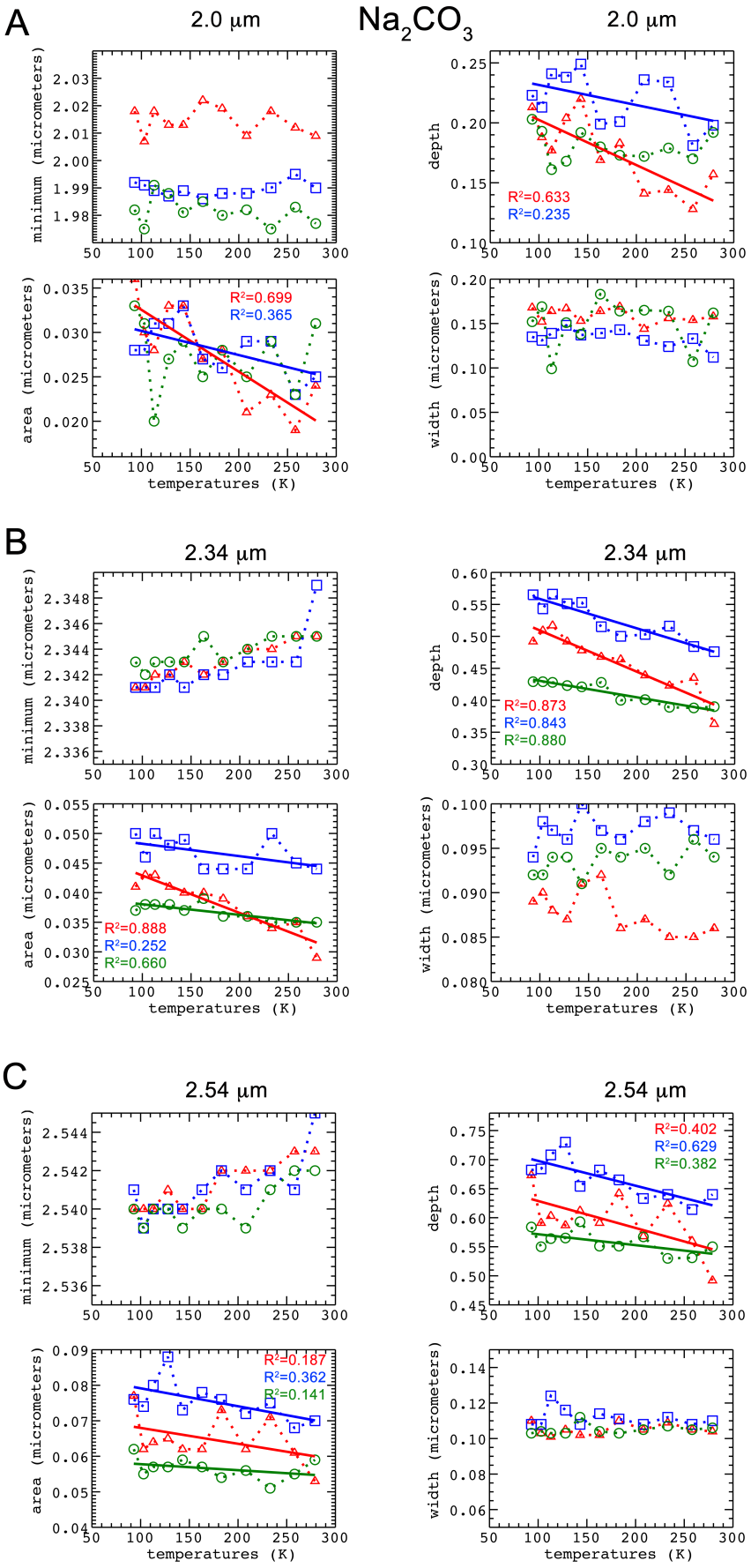

Figure 5. Na_2CO_3, band parameters of 2, 2.34 and 2.54-μm features. Red triangles: 36-50 μm. Blue squares: 75-100 μm. Green circles: 125-150 μm.

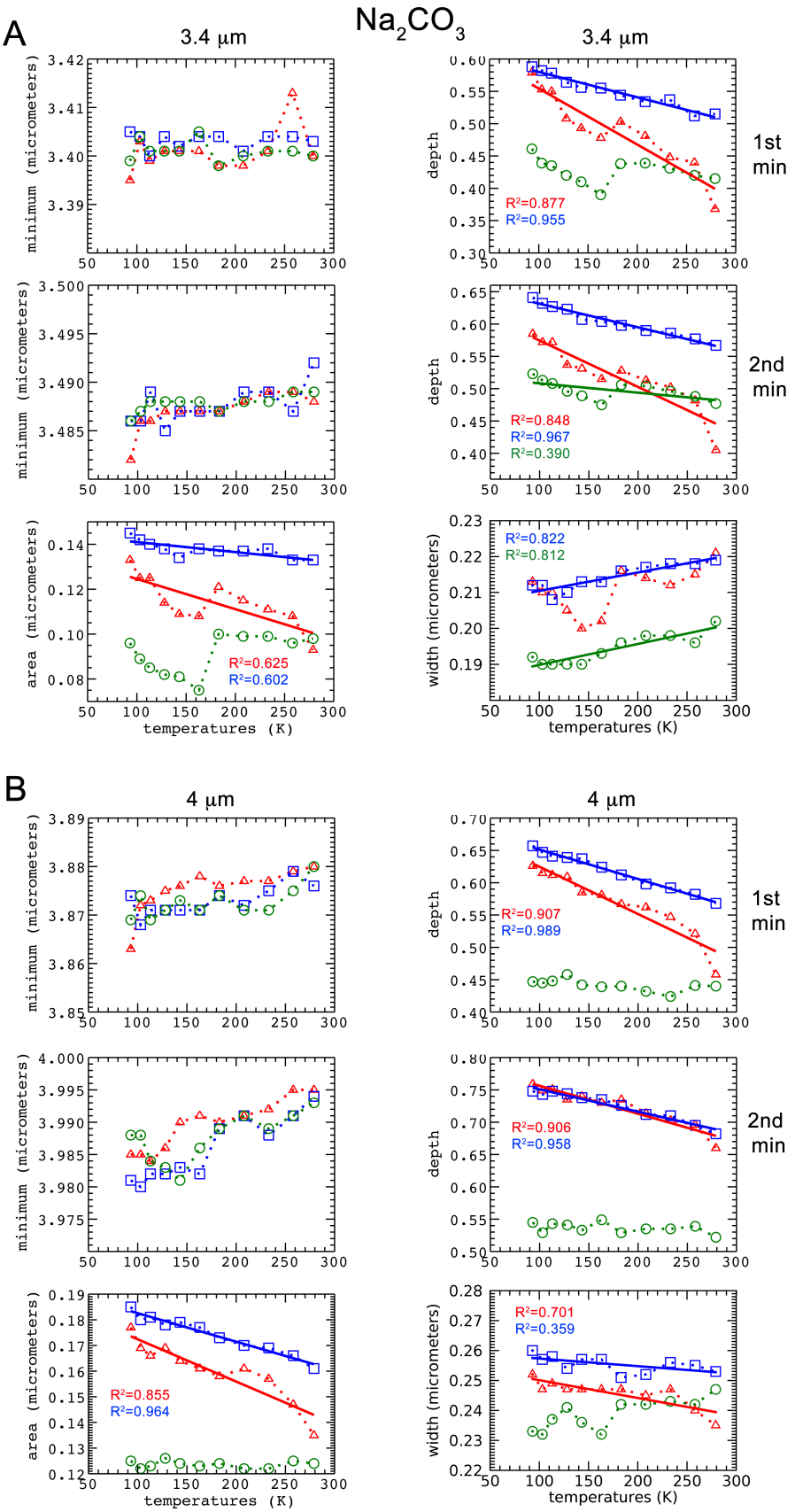

Figure 6. Na_2CO_3, band parameters of 3.40 μm (I) and 3.49 μm (II), and 3.88 μm (I) and 3.99 μm (II) features. Red triangles: 36-50 μm. Blue squares: 75-100 μm. Green circles: 125-150 μm.

3.4 Sodium carbonate monohydrate (thermonatrite)

3.4.1 1.57-μm band

The spectral indices of the 1.57-μm water absorption feature are shown in Fig. 7A. The band position shifts towards longer wavelengths by as much as ~20 nm (1.56-1.58 μm) as the temperature decreases. Both the depth and area linearly increase, by about 70-75%, towards low temperatures, becoming very definite and intense. The bandwidth shows a clear and systematic decrease with decreasing temperature, i.e. the band gets narrower, for all the three grain sizes. At 93 K the fine grain size (36-50 μm) presents the maximum band depth. This is true for the 1.57-μm band as well as for all other features occurring in the monohydrate sample.

3.4.2 1.78-μm band

Spectral indices are shown in Fig. 7B for the 1.78 μm feature. The first three parameters show trends similar to the previous band. The band position shifts towards longer wavelengths by about 20-30 nm (1.77-1.80 μm) while the temperature decreases. The band depth and area are both subject to a strong increase (more than 100%) as the temperature drops down. The bandwidth slightly increases towards lower temperatures, for all of the three grain sizes.

3.4.3 1.96-2.2 μm band complex

The 2-μm feature (Fig. 8) is likely due to the combination H_2O and CO_3^{2-} absorptions occurring in the same spectral region. This happens because in sodium carbonate monohydrate the CO_3^{2-} ions are bonded to H_2O molecules through hydrogen bonding (Farmer et al., 1974). In room temperature spectra (Fig. 2) this feature, with shorter and longer wavelength edges at 1.89 and 2.24 μm respectively, is composed of three separate minima, located at 1.96 (I), 2.06 (II) and 2.2 μm (III). These three relative minima become more defined (V-shape) and intense (larger depth) as the temperature decreases towards cryogenic values. The position of feature I (Fig. 8A) and also the position of feature II (Fig. 8B) shift as the temperature decreases towards shorter wavelengths (1.961-1.957 μm, about 4 nm, and 2.067-2.056 μm, about 11 nm, respectively; the latter is slightly above our spectral sampling). Both features are characterized by an increasing depth, by more than a factor of 2, as the temperature drops down to cryogenic values. The feature III displays an inverse shift, the position moves towards longer wavelengths (2.187-2.201 μm, about 14 nm, Fig. 8C) for lower values of temperature. The band depth of feature III also becomes even more intense as the temperature decreases. The area of the whole 2-μm band increases linearly towards cryogenic temperatures, while the width decreases, notably for the 75-100 and 125-150-μm grain sizes.

3.4.4 2.3-2.5-μm band complex

In room temperature spectra, this feature appears as a single asymmetric broad band located at 2.47 μm, with a shoulder on the left side near 2.4 μm. At cryogenic temperatures the fine structure of the band becomes evident, with three well-defined narrow features occurring approximately at 2.32 μm (I), 2.44 μm (II), and 2.50 μm (III). The feature III is well visible in all spectra in the range 93-279 K, the feature I appears clearly below 233 K, and the feature II is clearly discernible only below 183 K. The band parameters are shown in Fig. 9. The position

559 of feature I displays a shift towards shorter wavelengths by about 5-10 nm (2.333-2.321 μm),
560 depending on the grain size, as the temperature decreases, while the depth increases by more
561 than a factor of 3 (Fig. 9A). This value is comparable with our spectral sampling, but is below
562 our spectral resolution. Similarly, the feature II shifts towards shorter wavelengths of as much
563 as 20-40 nm (2.47-2.43 μm), and the corresponding band depth increases by more than 50%
564 (Fig. 9B) while the temperature drops down. The feature III shows an opposite behavior, with
565 its position having a shift towards longer wavelengths by 20-35 nm (2.47-2.505 μm); the
566 depth again increases at lower temperatures (Fig. 9C). The area of the whole 2.3-2.5-μm band
567 becomes larger by more than a factor of 2 with decreasing temperature. The band width is
568 calculated as full width half maximum, due to the fact that this band splits in several minima,
569 which poses some difficulty in computing an unambiguous parameter. Compared to the
570 previous spectral parameter, this one does not seem to display any strong correlation with
571 temperature.
572
573 *3.4.5 3-μm band*
574
575 The position of the 3-μm water absorption band (around 2.9 μm) is characterized by a shift
576 towards longer wavelengths by 20-30 nm, especially for the 36-50 and 75-100 μm grain sizes,
577 as the temperature decreases (Fig. 9D). This band is almost saturated in 125-150 μm spectra,
578 therefore the retrieved positions are not strongly correlated with temperature for the coarse
579 grains (Fig. 9D, green circles). An analogous behavior is displayed by the bandwidth: it slightly
580 increases for lower temperatures and for the 36-50 and 75-100 μm grain sizes, whereas no
581 substantial correlation is seen for the coarse grain size. The band depth and area increase
582 clearly and linearly as the temperature decreases.
583

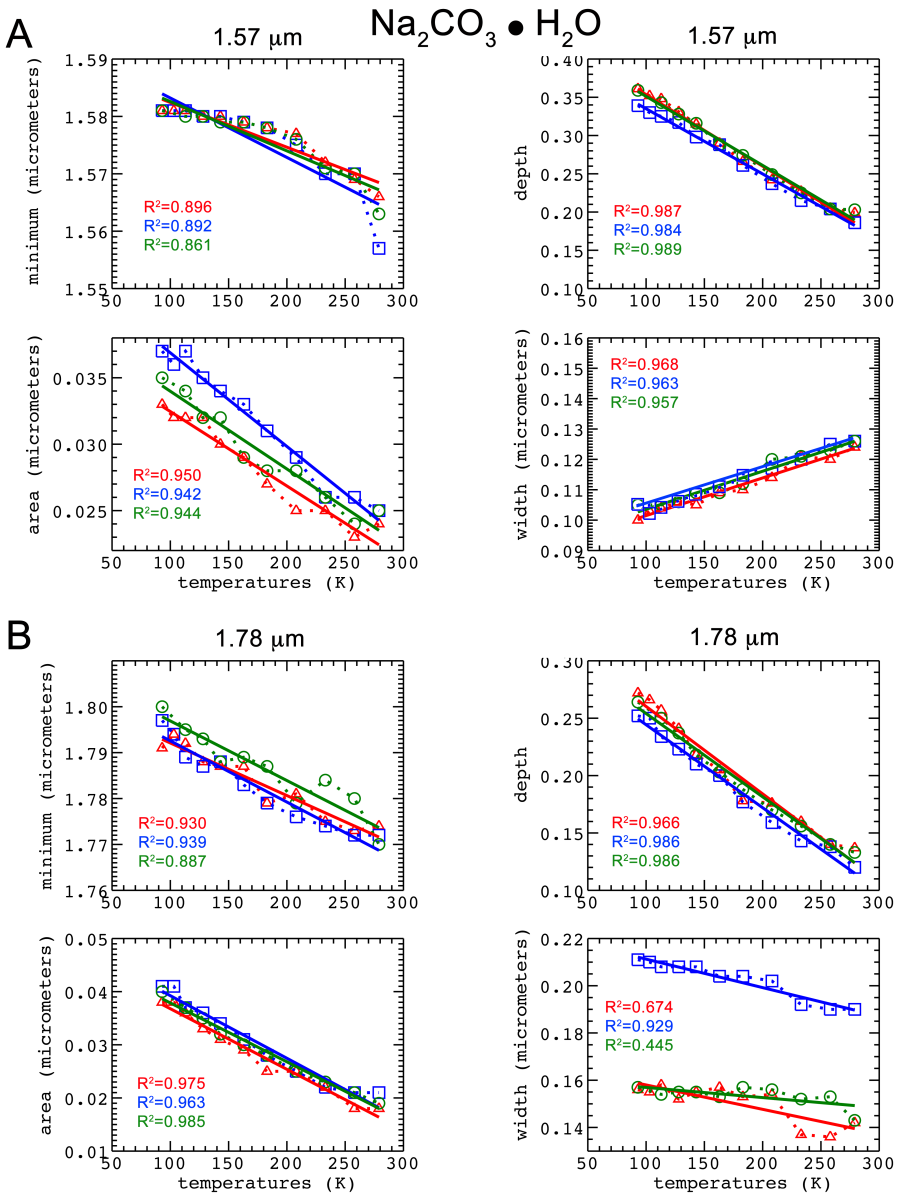

Figure 7. Na_2CO_3•H_2O band parameters of 1.57-µm and 1.78-µm features. Red triangles: 36-50 µm. Blue squares: 75-100 µm. Green circles: 125-150 µm.

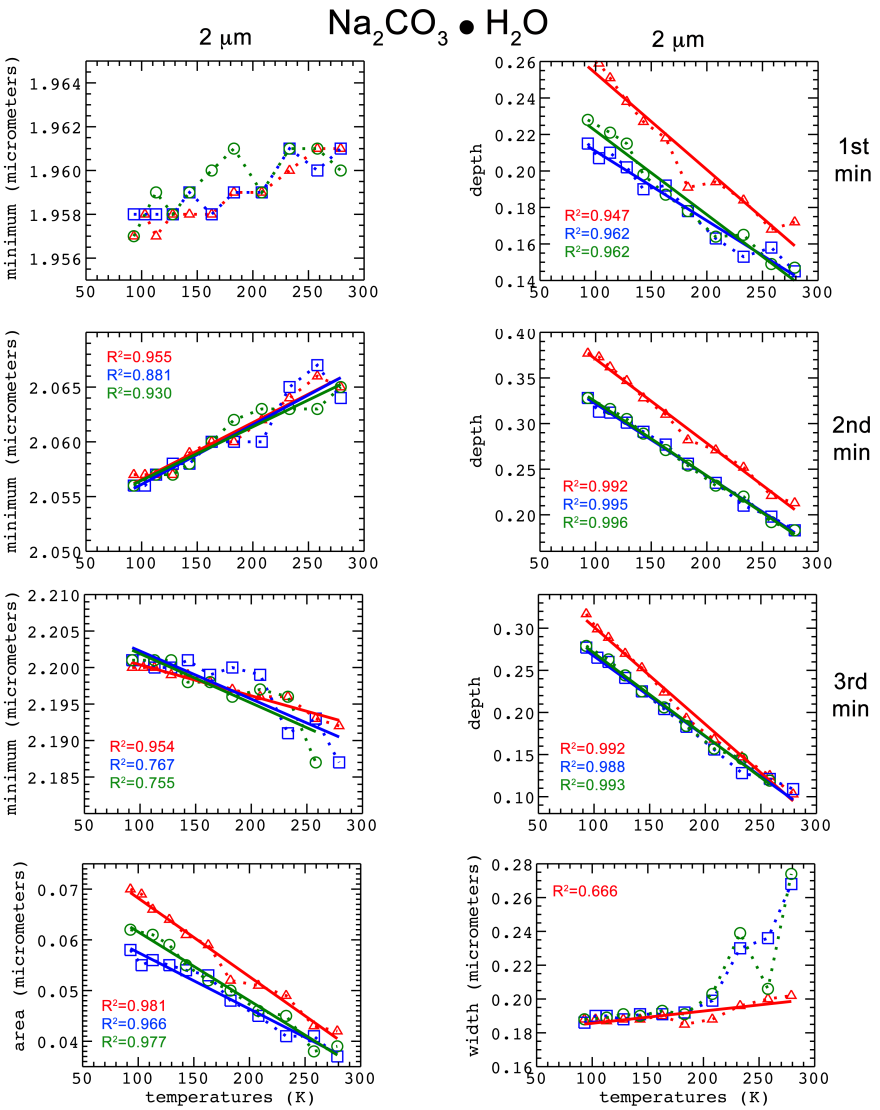

Figure 8. $Na_2CO_3 \bullet H_2O$ band parameters of 1.96 µm (I), 2.06 µm (II) and 2.20 µm (III) features. Red triangles: 36-50 µm. Blue squares: 75-100 µm. Green circles: 125-150 µm.

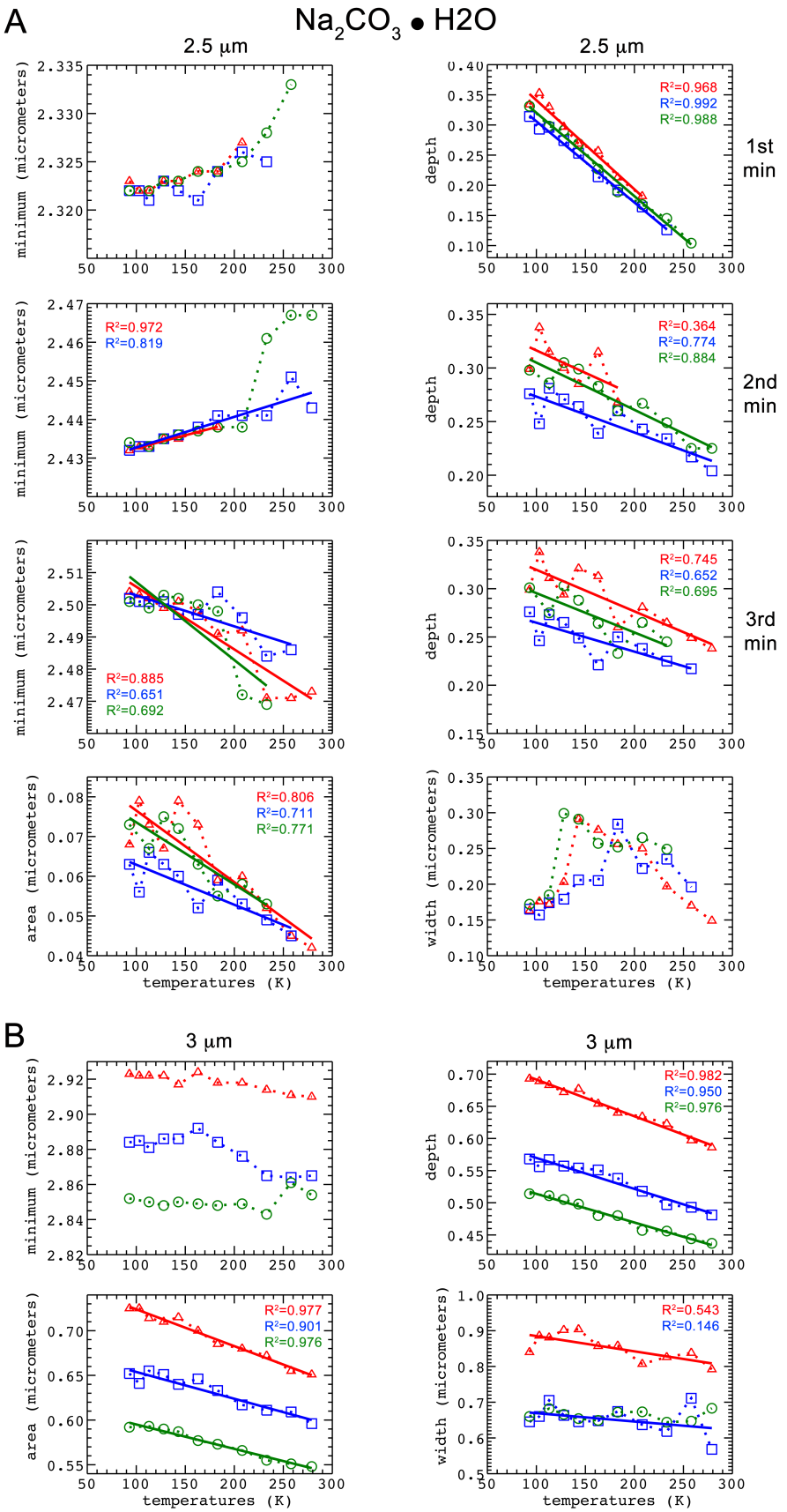

Figure 9. Na_2CO_3•H_2O band parameters of 2.32 μm (I), 2.44 μm (II) and 2.50 μm (III) features and 3.0-μm band. Red triangles: 36-50 μm. Blue squares: 75-100 μm. Green circles: 125-150 μm.

3.5 Sodium carbonate decahydrate (natron)

3.5.1 1.23-μm band

The water absorption at 1.23 μm shows dependencies from the temperature, as seen in Fig. 10A. The position shifts linearly towards longer wavelengths, by 20-30 nm, as the temperature decreases (1.215-1.245 μm). The depth and area also display an increase for lower temperatures, although with more fluctuations. The bandwidth does not show a clear correlation with temperature. The band depth also increases linearly with grain size from fine to coarse.

3.5.2 1.5-μm band complex

The 1.5-μm water band at room temperature occurs with a main minimum near 1.5 μm and a secondary minimum near 1.58-1.65 μm. This secondary minimum is more pronounced in finer grained size spectra and becomes a shoulder in coarser spectra (Fig. 3). At cryogenic temperature the band displays a fine structure, being composed by three minima located at 1.50 (I), 1.65 (II) and 1.75 μm (III). Here we analyzed only the features I and II, the third minimum being too weak and poorly resolved. The position of band I shifts towards longer wavelengths (1.485-1.505 μm) as the temperature decreases from 279 K to 93 K, and the depth increases by about 20%. The band II also shifts to longer wavelengths (1.58-1.65 μm) with decreasing temperature in the range 279-93 K, for the 36-50-μm grain size; it becomes visible only below 200 K for the 75-100-μm grain size, and below 150 K for the 125-150-μm grain size. The depth also increases with decreasing temperature, by 65% for the finest class. Finally both area and width, with respect to the whole 1.5-μm feature, display a strong increase towards lower temperatures. The band depths at 1.5 and 1.65 μm both increase with grain size, attaining the maximum values for the coarse grains.

3.5.3 2-μm band

The 2-μm band appears as a unique broad band in the whole temperature range 93-279 K. All spectral indices reported in Fig. 11A display a strong correlation with temperature. The band position shifts towards longer wavelengths by about 20-25 nm (1.97-2.00 μm) with decreasing temperature. The band becomes even more intense (increasing depth), broad and wide as the temperature decreases. This band shows an opposite behavior with respect to the previous bands: the smaller the grain size (36-50 μm), the greater the depth.

3.5.4 2.45-μm band

The band parameters of the 2.45-μm absorption, likely related to CO_3^{2-}, are shown in Fig. 11B. The position of this feature shifts towards shorter wavelengths by 15 nm (2.455-2.440 μm) with decreasing temperature. The band depth and area both increase by more than a factor 2 as the temperature decreases. Similarly to the 2-μm band above, the maximum depth for this band also occurs for fine grains. The bandwidth becomes broader for lower temperatures, although the rate of broadening decreases for decreasing grain size.

3.5.5 3-μm band

In Fig. 11C we show the band parameters for the 3-μm water absorption feature. The position displays a negative correlation with temperature (moving towards longer wavelengths as the temperature decreases, by 20-30 nm) notably for the 36-50 and 125-150-μm grain sizes. However, this strongly saturated band is characterized by a very broad and flat minimum, so a large uncertainty is associated to the retrieved central wavelength. The depth and area both increase with decreasing temperature. For a fixed temperature, area and depth assume larger values for the smallest grains size (36-50 μm) and clearly decrease moving to the medium and coarse grain size. The bandwidth displays different trends for the three grain sizes, although with large fluctuations. Concerning the dependence on grain size, the 3-μm water band depth again decreases linearly with increasing grain size.

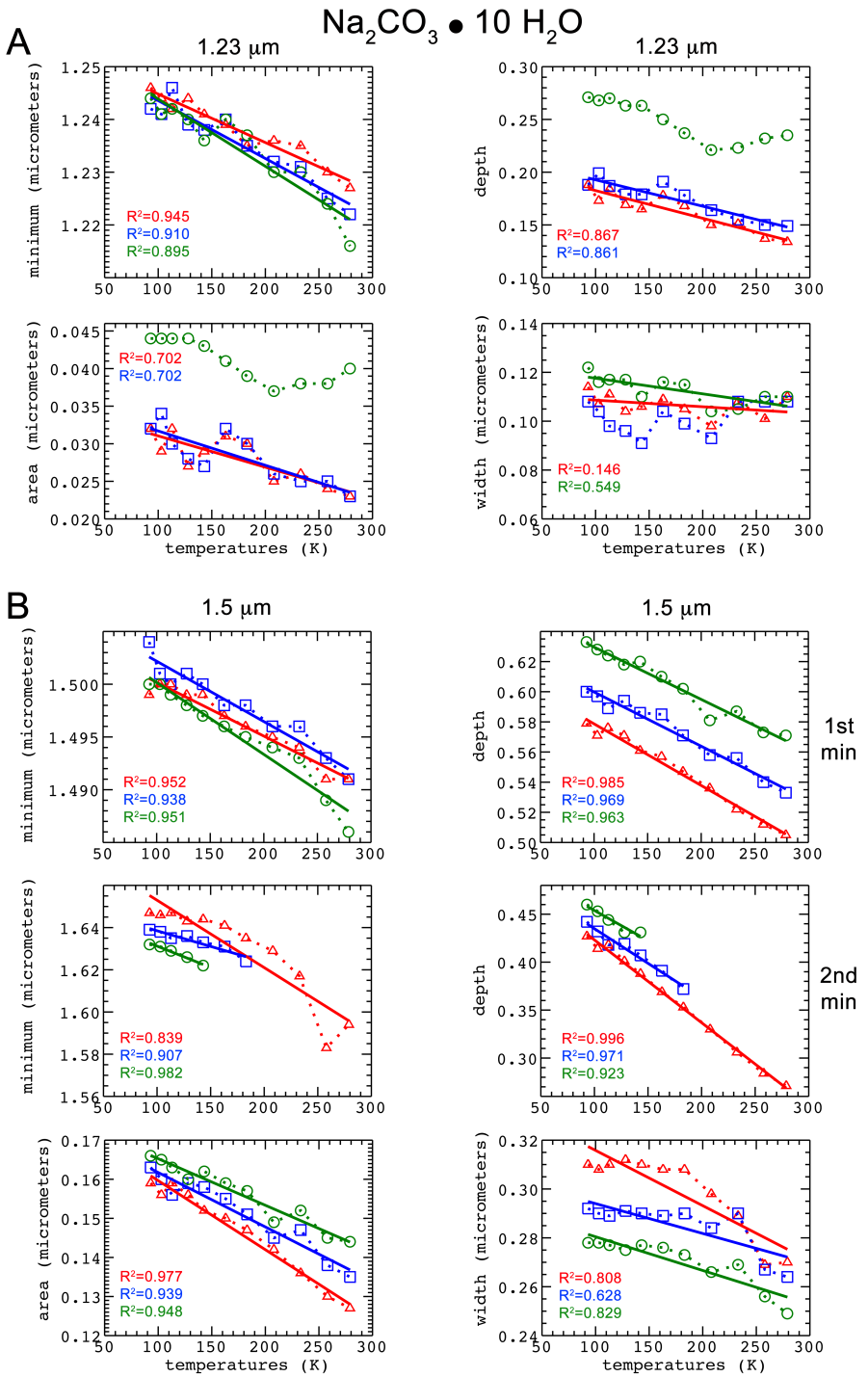

Figure 10. Na_2CO_3•10H_2O band parameters of 1.23-μm, 1.50 μm (I) and 1.65 μm (II) features. Red triangles: 36-50 μm. Blue squares: 75-100 μm. Green circles: 125-150 μm.

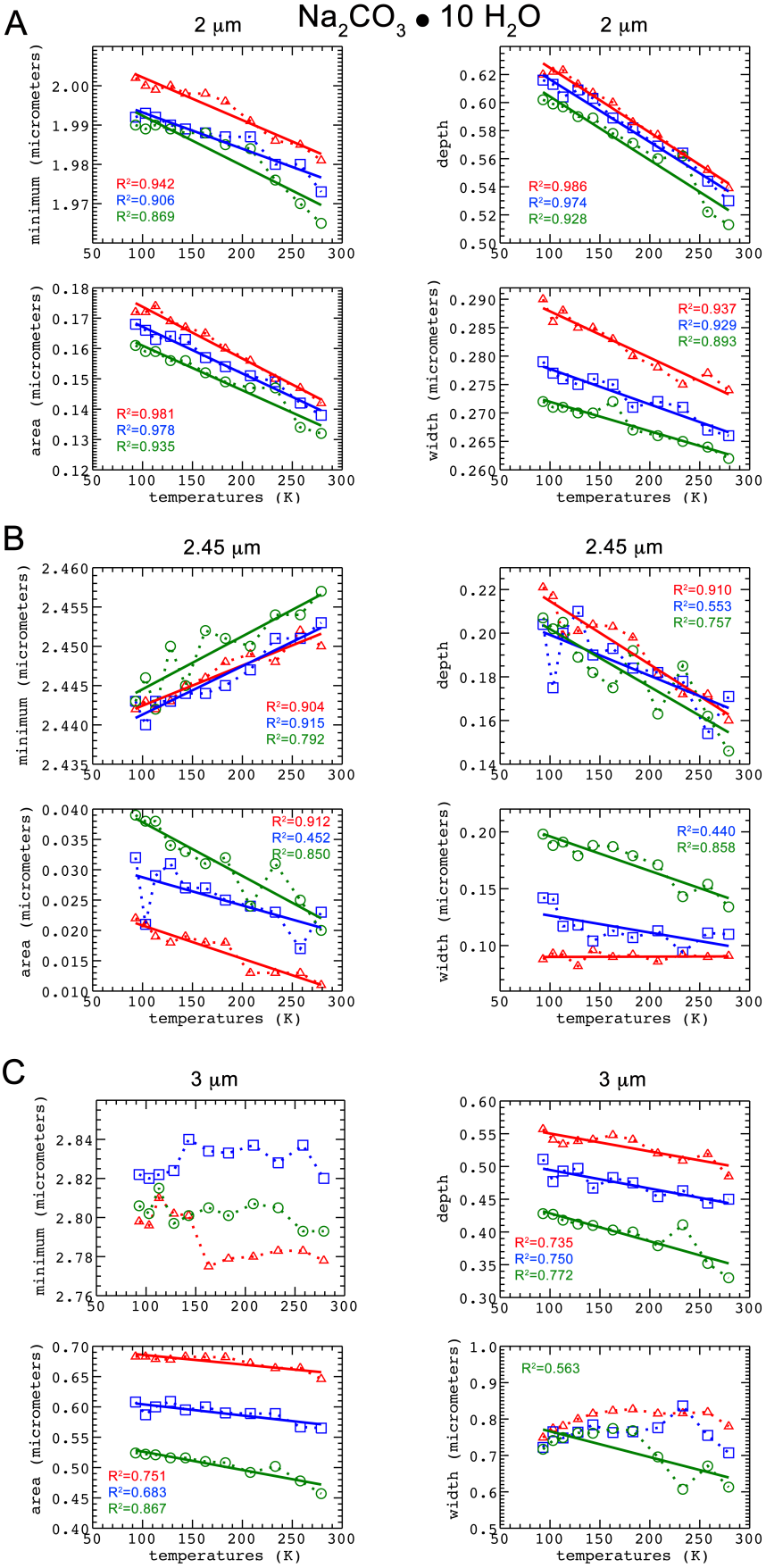

Figure 11. Na_2CO_3•$10H_2O$ band parameters of 2.0-μm, 2.45-μm and 3.0-μm features. Red triangles: 36-50 μm. Blue squares: 75-100 μm. Green circles: 125-150 μm.

669 # 4. Discussion
670
671 ## 4.1 Natrite carbonate bands at 3-4 μm
672
673 The 3.4- and 4-μm carbonate bands of natrite, both characterized by two close narrow
674 minima, show a change in relative intensity as a function of temperature. One explanation for
675 doublet bands (with split minima) is that a coupling of vibrational modes, related to different
676 molecular ions located in equivalent (symmetric) sites in the unit cell, can occur (Brooker &
677 Bates, 1971). Another explanation is the "two-site effect", in which a particular group (for
678 example the CO_3^{2-} ion) occupies two different sites (Brooker & Bates, 1971). Here we find that
679 the relative strength of double minima of each band changes with temperature. We computed
680 the band depth ratios of the two minima of each band: the 3.4-μm band has two minima, I and
681 II, respectively centered near 3.40 and 3.49 μm, while the 4-μm band has two minima, I and II,
682 centered near 3.88 and 3.99 μm, respectively. The depth ratios are given by:
683

$$BR_{3.4} = \frac{Bdepth_{3.40}}{Bdepth_{3.49}}$$

684

$$BR_{4.0} = \frac{Bdepth_{3.88}}{Bdepth_{3.99}}$$

685
686 The retrieved band depth ratios are shown in Fig. 12. The band depth ratio for 3.4 μm band
687 minima (Fig.12A) shows a slightly different behavior as a function of temperature, depending
688 on the grain size. Starting from room temperature, the depth ratio displays an increase
689 towards low temperatures, especially for the 36-50 μm grain size. The depth ratio rate tends
690 to reduce as the grain size becomes coarser. However this may not be an intrinsic behavior,
691 because for the coarser grain size (125-150 μm) the 3.4-μm band shape could be substantially
692 affected by the 3-μm water absorption; this is due to some adsorbed water on the grains of
693 the anhydrous sample. The depth ratio for the 4-μm band shows a more consistent behavior.
694 In all of the three grain sizes, the ratio displays a net increase as the temperature goes down
695 from 279 K to 93 K. A general explanation could be that the changes observed in band depths
696 and band depth ratios are due to changes in the reflectance of the spectral continuum (where
697 the continuum is drawn) with temperature and grain size. The effect on the continuum could
698 be enhanced when viewing at close bands (such as 3 and 3.4 μm).
699

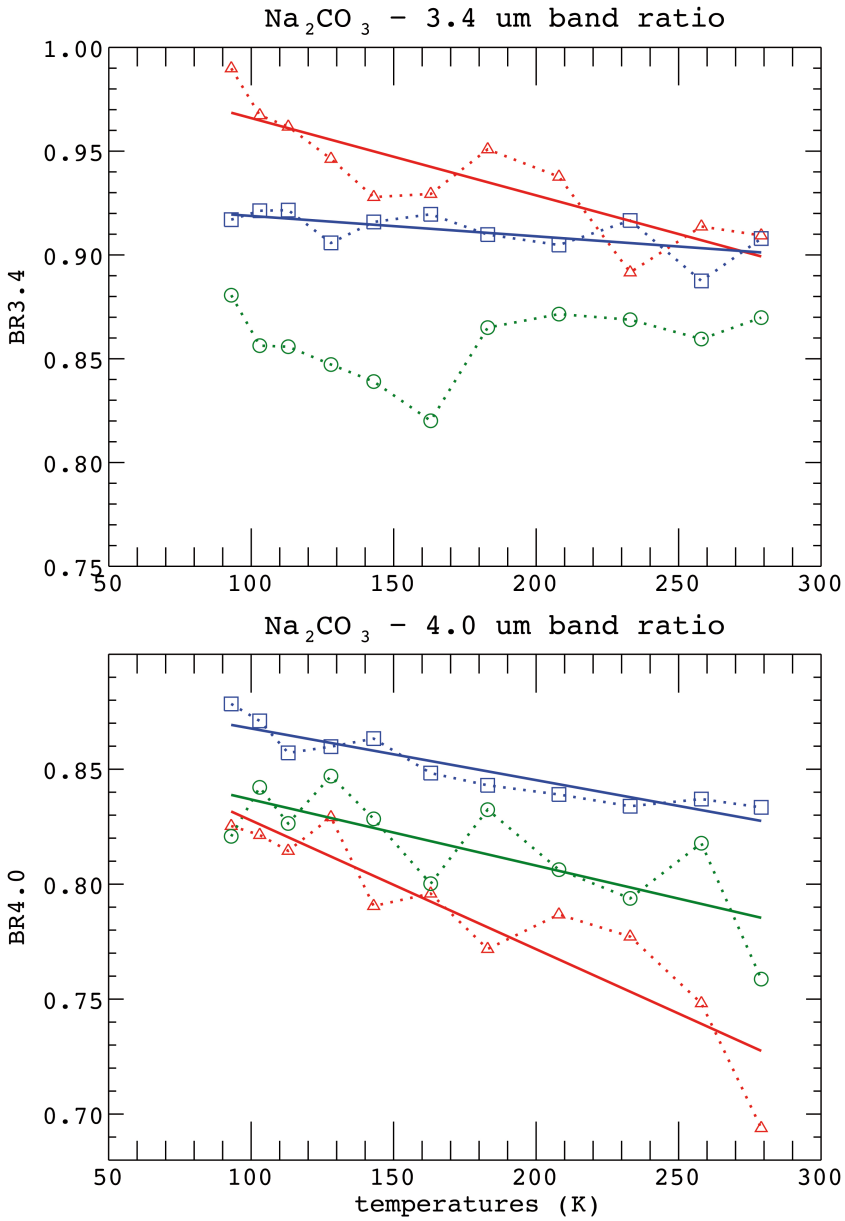

Figure 12. Natrite, band depth ratios for relative minima of carbonate bands. A: 3.4 micron band. B: 4.0 micron band. Red triangles: 36-50 μm. Blue squares: 75-100 μm. Green circles: 125-150 μm.

4.2 Differences between hydration bands among thermonatrite and natron

The spectra of the three analyzed compounds appear markedly different in terms of bands shapes and positions. The main differences among them occur between the hydration absorption bands, specifically for thermonatrite ($Na_2CO_3 \bullet H_2O$) and natron ($Na_2CO_3 \bullet 10H_2O$). The less hydrated species, thermonatrite, at room temperature displays numerous narrow absorption bands that tend to become separate in even more and narrower features at cryogenic temperatures. All these features reflect the energy levels corresponding to the possible vibration states of the H_2O molecule. Nevertheless the features (energies) tend to remain separate because of the low number of water molecules. In the heavily hydrated species, i.e. natron, a higher number of energy levels is the result of many vibrational states allowed for the numerous (10) water molecules per structure unit. Furthermore, the cohesive

718 forces in the crystal lattice are mainly due to the hydrogen bond (Buijs & Schutte, 1961b).
719 This in turn produces a few broad and large absorption bands, especially at 1.5 and 2 μm,
720 constituted by the overlapping/combination of numerous undistinguishable features (Farmer
721 et al., 1974). Finally, as pointed out by Buijs & Schutte (1961b), the 3-μm band in
722 monohydrate is likely most related to carbonate–water hydrogen bonding, while the 3-μm
723 band in decahydrate is mostly due to water–water hydrogen bonding.
724
725 4.3 Hydration state and 3-μm band variability
726
727 The increasing level of hydration in the sequence natrite → thermonatrite → natron (0 → 1 →
728 10) also implies clear changes in the 3-μm spectral region of water absorption. In Fig. 13A we
729 show the 279 K and 93 K spectra for the three samples at 36-50-μm, for direct comparison.
730 Three more factors characterize the sequence of hydration, beyond the already discussed
731 absorption bands: (i), a shift towards shorter wavelengths of the 3-μm band position, (ii) a
732 decrease of the overall reflectance, and (iii) a progressive increase in the NIR slope (1-2.5 μm;
733 negative) as the number of water molecules increases. The 3-μm band position has been
734 computed for each species, averaged among the three grain sizes and plotted against the
735 number (N) of H_2O molecules (Fig. 13B); error bars are obtained by calculating the standard
736 deviation after varying the band edges for continuum removal. The position clearly shifts
737 towards shorter wavelengths as the water content of the species increases. The spectral
738 continuum has been retrieved at 2.6 μm, following the same approach as for the 3-μm
739 position; this parameter is plotted as a function of water molecules in Fig. 13C. The continuum
740 reflectance level is characterized by a net decrease as the water content of the mineral
741 increases. Finally the NIR slope has been computed in the range 1-2.5 μm. The absolute value
742 of the slope displays a net increase (the negative slope decreases) as the number of water
743 molecules increases (Fig. 13D).
744 A narrow minimum at 3.1 μm in natrite, which does not show up in the starting 279 K-
745 spectrum (Fig. 1, red line, bottom) appears in the 93 K-spectrum (orange line) and then
746 weakens and disappears as the temperature increases up to 279 K (red line, top). This
747 absorption could be due to the formation of some very finely grained water frost on the
748 sample. In the 75-100-μm grain size spectra the appearing and disappearing of two minima at
749 2.99-3.1 μm at the lowest temperatures could be evidence of the same phenomenon. In
750 general, in the 3-μm region of thermonatrite and natron, we observe a global change, as
751 discussed, mainly consisting in the reduction of the reflectance level at cryogenic
752 temperatures and in the formation of a well defined large absorption band; this is as also
753 evidenced by the more pronounced shape of the 3.75-μm reflectance maximum, whose
754 position shifts towards shorter wavelengths, while the 2.75-μm position shifts in the opposite
755 direction (e.g. Fig.12A). The general narrowing of the whole band as the temperature
756 decreases is consistent with a lower number of allowed vibrational modes (due to changes in
757 thermal population) at cryogenic temperatures.
758

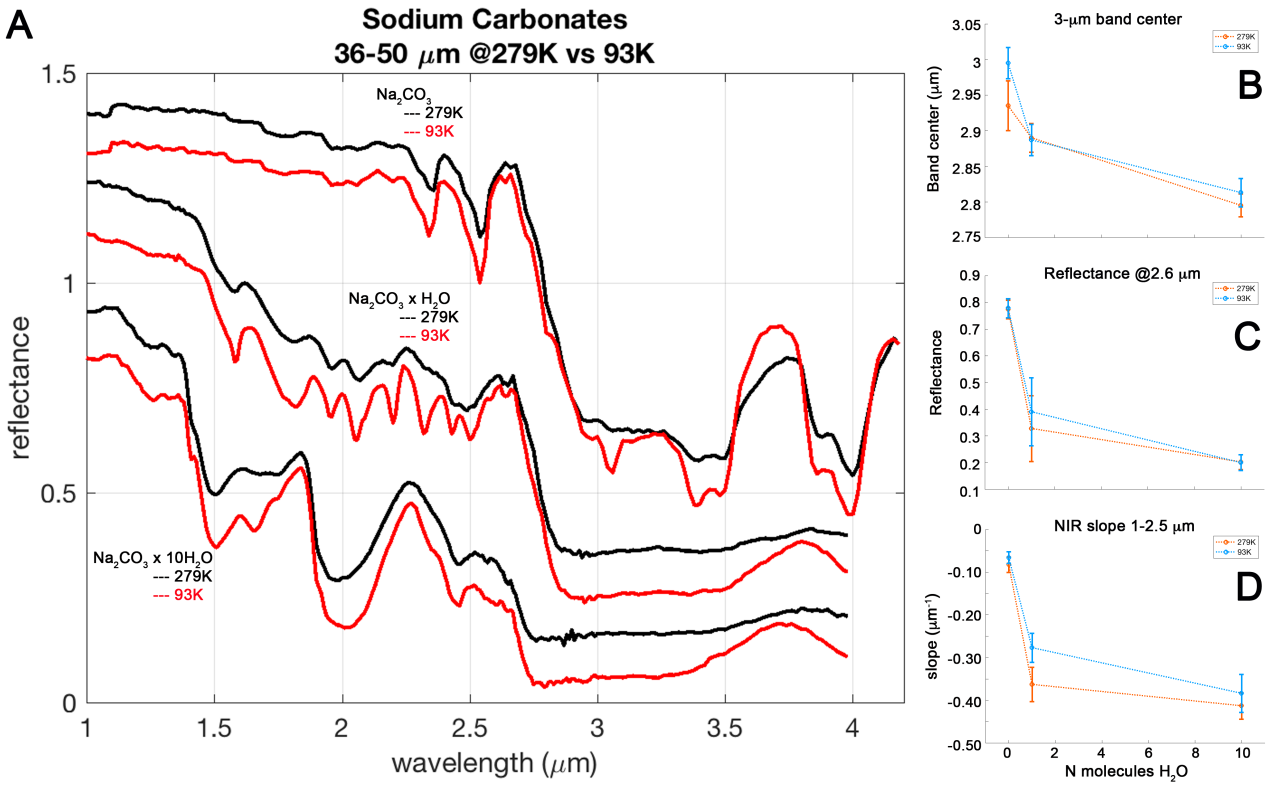

Figure 13. A. Spectra acquired for the three species for 36-50 μm grain size, at 279 K (black) and 93 K (red). Spectra of Na_2CO_3 and Na_2CO_3•H_2O are shifted in reflectance by 0.2 and 0.1 for clarity, respectively. B. Band minimum of the 3 μm band, as a function of number of water molecules. C. Reflectance @2.6 μm as a function of water molecules. D. NIR slope (1-2.5 μm) versus water molecules. For each specie, the spectral parameters have been averaged over the three grain sizes.

4.4 Temperature dependence of H_2O and CO_3^{2-} species.

Table 2 schematically synthesizes with arrows the behavior of each analyzed parameter, as a function of decreasing temperature. For all the absorption features, regardless of the originating chemical species, the depth and area increase as the temperature decreases. The bandwidth does not display a unique behavior, mainly because it is difficult to define an unambiguous width parameter for multi-minima and fine structured bands. The band minimum displays the following behavior: the band minimum regularly shifts towards shorter wavelengths, as the temperature decreases, when related to CO_3^{2-} vibrations; on the contrary the minimum appears to shift towards longer wavelengths when the band is assigned to H_2O transitions. The H_2O transitions are mostly related to hydrogen bonds in water–water interactions. The strength of hydrogen bond increases as the temperature decreases, and its effect is to shift the band minimum towards lower frequencies (longer wavelengths). In some cases the behavior is mixed, that is relatively to overlapping absorption bands due to both H_2O and CO_3^{2-} (bands with fine structure at 2.0 and 2.5 μm in thermonatrite). Our finding of CO_3 absorption shifting towards shorter wavelengths (higher wavenumbers) as temperature decreases however is consistent with the results of Harris & Salje (1992), and can be explained with an increasing and strengthening of CO_3–Na interactions, as discussed above (Harris & Salje, 1992; Arakcheeva & Chapuis, 2005). Concerning the shift in position of H_2O transition features, instead, our opposite results are consistent with findings of Grundy & Schmitt (1998). They found, in Near-IR transmission

spectra of water ice, that H_2O absorptions move towards longer wavelengths with decreasing temperature.

Sample	*B (μm)*	*Absorption*	*B_C vs decreasing T*	*ΔB_C*	*B_D vs decreasing T*	*ΔB_D*	*B_A vs decreasing T*	*ΔB_A*	*B_W vs decreasing T*	*ΔB_W*
Na_2CO_3	2.0				↑	+30%	↑	+75%		
	2.34	CO_3^{2-}	← (short λ)	-10 nm	↑	+43%	↑	+50%		
	2.54	CO_3^{2-}	← (short λ)	-4 nm	↑	+40%	↑	+33%		
	3.40 (I)	CO_3^{2-}			↑	+71%	↑	+40%	↓	-4.5%
	3.49 (II)	CO_3^{2-}	← (short λ)	-5 nm	↑	+50%			↓	-4.5%
	3.88 (I)	CO_3^{2-}	← (short λ)	-15 nm	↑	+44%	↑	+38%		
	3.99 (II)	CO_3^{2-}	← (short λ)	-15 nm	↑	+15%				
Na_2CO_3 •H_2O	1.57 (II)	H_2O	→ (long λ)	+25 nm	↑	+75%	↑	+60%	↓	-23%
	1.78	H_2O	→ (long λ)	+30 nm	↑	+116%	↑	+100%	↑	+10%
	1.96 (I)	H_2O+CO_3^{2-}	← (short λ)	-3 nm	↑	+62%	↑	+75%	↓	-36%
	2.06 (II)	H_2O+CO_3^{2-}	← (short λ)	-10 nm	↑	+100%				
	2.20 (III)	H_2O+CO_3^{2-}	→ (long λ)	+15 nm	↑	+200%				
	2.32 (I)	H_2O+CO_3^{2-}	← (short λ)	-14 nm	↑	+200%	↑	+100%		
	2.44 (I)	H_2O+CO_3^{2-}	← (short λ)	-40 nm	↑	+35%				
	2.50 (III)	H_2O+CO_3^{2-}	→ (long λ)	+30 nm	↑	+28%				
	3.0	H_2O	→ (long λ)	+20 nm	↑	+17%	↑	+8%	↑	+12%
Na_2CO_3 •10 H_2O	1.23	H_2O	→ (long λ)	+20 nm	↑	+36%	↑	+33%		
	1.50 (I)	H_2O	→ (long λ)	+15 nm	↑	+16%	↑	+23%	↑	+17%
	1.65 (II)	H_2O	→ (long λ)	+60 nm	↑	+72%				
	1.99	H_2O	→ (long λ)	+25 nm	↑	+15%	↑	+23%	↑	+5.5%
	2.45	CO_3^{2-}	← (short λ)	-15 nm	↑	+37%	↑	+100%	↑	+30%
	3.0	H_2O	→ (long λ)	+10 nm	↑	+31%	↑	+15%		

Table 2. Band parameters variations (vs temperature decrease) for the analyzed spectral features. Abbreviations are: B = band, B_C = band position, B_D = depth, B_A = area and B_W = width. Maximum percent changes are listed in columns on the left side of each corresponding parameter.

4.5 Variations with grain size

In Fig. 14 we show the band depths at 93 K for each sample and for all of the considered grain sizes. The band depth displays a different behavior, as a function of grain size, for the different types of samples. Concerning the anhydrous sample (natrite, Fig. 14, top) the band depth value reaches a maximum at intermediate grain size (75-100 μm) for nearly all the absorption bands. In the monohydrate sample (Fig. 14, center) the band depth assumes maximum values for the fine grain size (36-50 μm), in all the absorption bands except the 3-μm band. Finally, regarding the decahydrate sample (Fig. 14, bottom) the band depths at 1.23, 1.50 and 1.65 μm increase with increasing grain size, while the band depths at 1.96-2.20, 2.45 and 3 μm decrease with increasing grain size. It has to be noted that the 3-μm feature has the same behavior (maximum BD for fine particles) for mono- and decahydrate: this is because this water feature readily saturates also for fine particles. The general behavior is explained considering that different materials (and different absorption features) are characterized by optimal grain sizes that maximize the absorption relative to the nearby continuum levels and the corresponding band depth (Hapke, 1993; Harloff & Arnold, 2001). When the grain size increases, first the reflectance at band center decreases faster than its continuum, then the band starts to saturate and the spectral continuum in between two bands decreases faster than the one at band center. The onset between these two behaviors occurs at lower grain size for stronger bands. However, overlapping of band wings may modify this general

behavior. Thus, in the anhydrous sample a "critical" grain size is reached at 75-100 μm. In the decahydrate sample, this is the grain size at which the band depth reaches its maximum value, decreases as passing from weak absorptions (1.23 μm) to more intense absorptions (i.e. towards the 3-μm band) (Hapke, 1993). In the case of monohydrate sample, the situation is complicated by the high concentration of closely spaced absorption bands and by the fact that absorption features are complex combinations of CO_3^{2-} and OH^-/H_2O transitions.

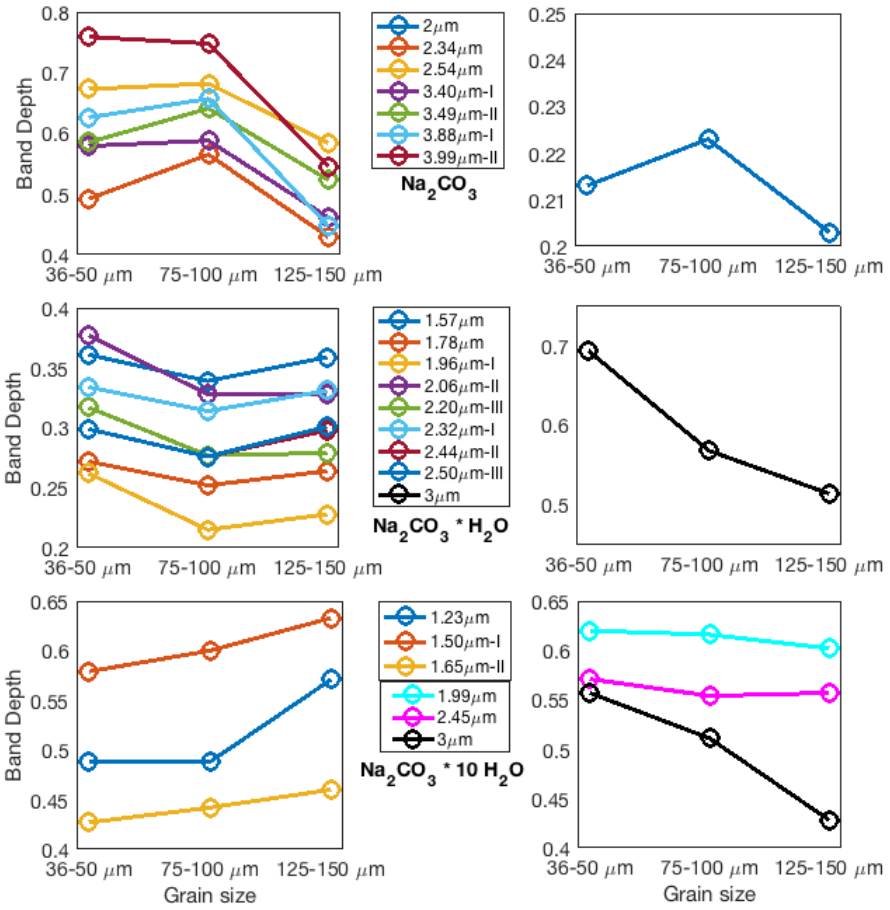

Figure 14. Band depth values at 93 K for the absorption bands of the three samples, as a function of the sample grain size. Top: natrite. Center: thermonatrite (monohydrate). Bottom: natron (decahydrate).

4.6 Comparison with Ceres

As discussed in Section 1, natrite has been invoked as the main component of some of the high-albedo geologic features observed on Ceres. Here we report a comparison of the 3-4-μm region between Dawn-VIR spectra of Cerealia Facula, i.e. the brightest feature found in the middle of the floor of crater Occator (De Sanctis et al., 2016) and our natrite spectra. In particular, we compare the VIR-measured spectra of two locations within Cerealia Facula (hereafter BS1, BS2 from Raponi et al., 2018; Fig. 15), with five different spectra of medium grain-sized natrite acquired at 93, 143, 208, 233 and 279 K. In particular, this has been inferred observing the behavior of the 3.40 μm (I) and 3.49 μm (II) minima. The 3.40 μm (I) position shifts towards shorter wavelengths in the 93 K, 143 K and 208 K spectra, compared to the bright spot (red dotted line); the 3.49 μm (II) position shifts towards shorter wavelengths in the 93 K spectrum (red dotted line). The 233 K spectrum has both I and II positions matching the same positions of the BS1 and BS2 spectra (black dashed lines, located at 3.40 and 3.50 μm). From this analysis, given the shift in position as a function of

temperature, we can infer that a temperature around 230K can be associated with bright spots.

The shape of the 4-μm feature can further support this conclusion. At the three lowest temperatures in Fig. 15 (93, 143 and 208 K), the two minima at 3.88 and 3.99 μm in natrite spectra are clearly separated by a relative maximum. In the spectra of bright spots BS1 and BS2, instead, the 3.88-μm feature appears as a shoulder on the left side of the 3.99-μm minimum. The best matching spectrum, despite the difference in intensity, is the one acquired at 233 K, in which again the 3.88-μm feature appears as a shoulder of the 3.99-μm minimum.

The 279K spectrum has the short-wavelength minimum of the 3.4 μm band shifted at 3.38 μm; the short-wavelength side of the 4 μm band again appears as a separated minimum rather than as a shoulder.

The 233K temperature value is consistent with maximum daytime temperature values retrieved on Ceres by VIR using its long-wavelength region between 4.5 μm and 5.1 μm, where thermal emission from the surface dominates the measured signal (Tosi et al., 2016).

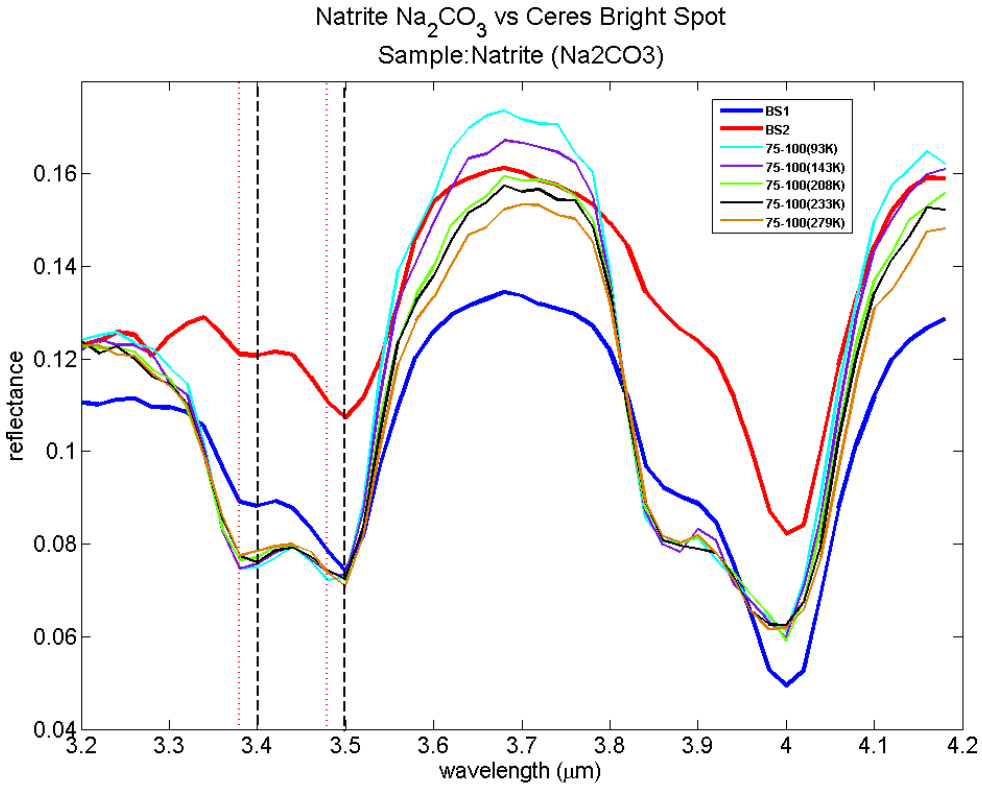

Figure 15. Spectra of Natrite sample with 75-100 μm grain size at 5 temperatures compared to two spectra of Ceres Bright Spots (BS1 and BS2). VIR data have been resampled on the same set of wavelengths used in the lab (the average VIR spectral sampling is ~10 nm in the infrared range 1-5 μm, De Sanctis et al., 2011). The two red-dotted lines indicate the positions of minima in the 93K spectrum. The two black-dashed lines indicate the positions of band minima of BS1 and BS2: they both match with the minima in the 233K spectrum.

4.7 Comparison with Europa

In Fig. 16 we compare four spectra of natron of intermediate grain size, respectively acquired at 93, 113, 163 and 208 K, to three spectra of Europa corresponding to as many locations observed by Galileo-NIMS (from McCord et al., 2010), and to pure water ice (fine snow, from ENVI spectral library) for reference. The spectra from McCord et al. (2010, Fig. 3b) refer to

different pixel areas: spectrum "A" is interpreted to be water ice-like, spectrum "D" in interpreted as heavily hydrated terrain, whereas spectrum "E" is an area intermediate between "A" and "D". From a comparison between our measurements and NIMS data it appears that our spectra display a better agreement with NIMS spectra labeled as "water ice-like" (spectrum A), or at least are intermediate between A and E. By looking at the 1.5-μm region, the 113-163 K spectra seem the most similar, given that the 93 K-spectrum displays too strong 1.75-μm feature, while the 208 K spectrum has a too weak 1.65-μm feature. However, in NIMS-measured spectra of Europa, water-related bands are shifted to longer wavelengths compared to our natron spectra, only slightly at 1.5 μm, but more clearly for the 1.25 and 2 μm bands. This, combined with a redder near-IR slope as observed in Europa, suggest that non-ice materials other than natron shoud be better candidates to fit the Europa spectra in the near infrared .

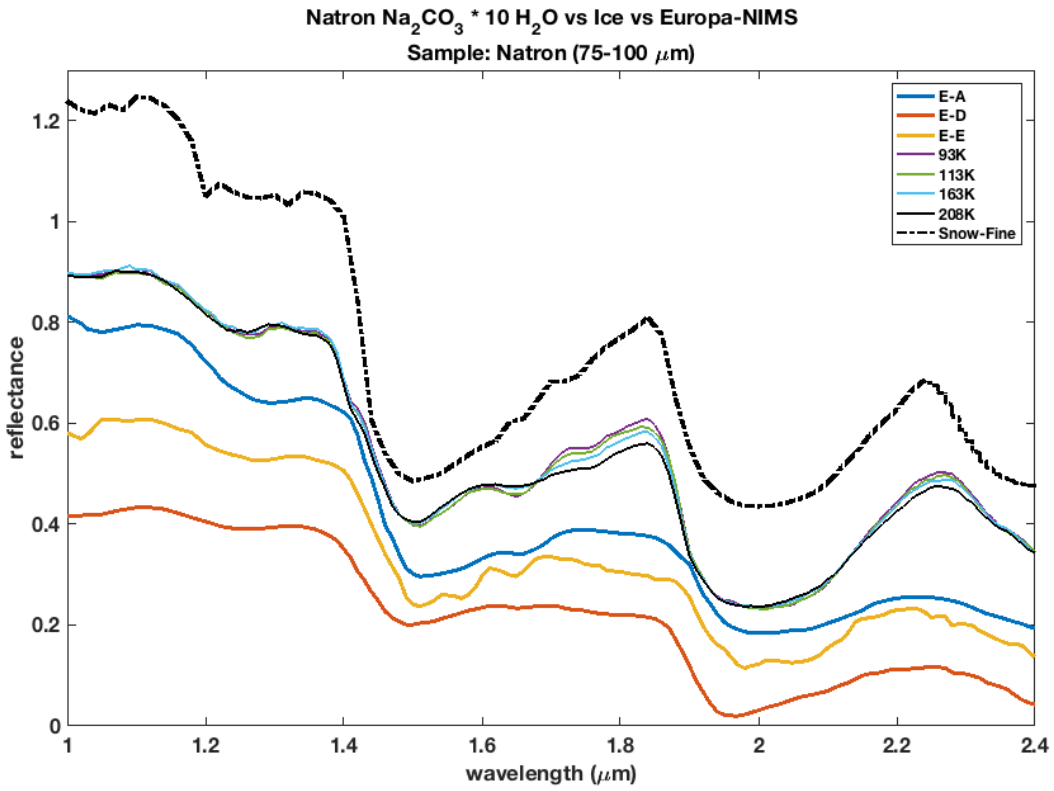

Figure 16. Laboratory spectra of natron with 75-100 μm grain size at four different temperatures, compared to three spectra of Europa-NIMS (From McCord et al., 2010; spectra pixel A, D, E) and with pure water ice (fine snow, ENVI JHU-Johns Hopkins University Spectral Library, Baldridge et al., 2009).

4.8 Implications for MAJIS-JUICE

The MAJIS spectrometer (Piccioni et al., 2014) onboard the ESA JUICE mission will observe Jupiter's moons in the 0.5-5.54-μm range, with unprecedented spectral sampling: on average, 3.6 nm/band in the 0.5-2.35-μm channel and 6.5 nm/band in the 2.25-5.54-μm channel. A legitimate question is whether this instrument in principle would be able to reveal the same temperature-dependent spectral changes we retrieved for the sodium carbonate samples. We focus on the absorption features that show the largest displacements in position.

Natrite:

- the bands at 2 and 2.35 μm show shifts by about 10 nm, that are comparable with our spectral sampling
- the 3.88 μm I and 3.99 II features show a shift in minimum of 10-15 nm, again comparable with actual spectral sampling, but well above the spectral detection threshold of MAJIS.

Thermonatrite:

- the band at 1.57 and 1.78 μm shift by 20-30 nm
- the 2.06 μm II band has a shift of about 10 nm; the 2.20 μm III band shifts by 8-14 nm
- the 2.5-μm bands display shifts of 5-11 nm, 20-35 nm and 20-35 nm, relatively to the three features at 2.32, 2.44 and 2.50 μm.
- the 3-μm feature minimum varies by about 15-20 nm.

Natron:

- the 1.23 μm band minimum varies by 20-30 nm
- the minimum of 1.5-μm band shifts by about 15 nm and 20-60 nm for the two occurring features at 1.50 and 1.65 μm
- minimum changes by about 20-25 nm and 15 nm relatively to 2-μm and 2.45-mm bands, respectively.

In the case of bright spots found on Ceres, whose surface composition sometimes is compatible with the presence of sodium carbonates, a direct comparison with our laboratory spectra allowed us to confirm that the anhydrous form (natrite) provides the best spectral match and to infer the temperature that provides the best agreement with the measured spectra.

In principle, temperature-dependent spectral shifts in sodium carbonates, if present on the surface of the icy Galilean moons, should be observable with JUICE-MAJIS. The most sensitive bands (~0.2 nm/K) may allow one to determine the surface temperature with an accuracy better than 10-15 K, provided that the material unit is in relatively pure form and the signal-to-noise ratio is large enough. Future comparisons with the band shapes and the relative band intensities may further improve this accuracy. Concerning the band intensity, the depth and area values for most of the bands vary by a minimum of 5-10% up to a factor of 2 or 3 for many absorption bands.

5. Conclusions

In this paper, we measured three sodium carbonates, i.e. natrite, thermonatrite and natron, in the infrared range 1-4.0 / 1-4.2 μm, in a range of cryogenic temperatures and in three different grain sizes, demonstrating that they show clear temperature-dependent behaviors. As the temperature decreases from 279 K down to 93 K, we can safely identify a number of spectral characteristics that are common to all the samples and grain sizes, namely:

- A fine structure of absorption bands appears and becomes more defined at lower temperatures. Some new features become visible at low temperatures, others increase their strength.
- The band depth and area values typically increase as the temperature decreases.
- The bandwidth show contrasting behavior, depending on the particular absorption band.

As the water content increases, in the sequence: natrite → thermonatrite → natron (0 → 1 → 10 H_2O molecules), we observe that:

- the 3-μm water absorption becomes more intense and saturates, and its short-wave wing moves towards shorter wavelengths: i.e., the saturation region becomes larger and starts at even shorter wavelengths as the water content increases.
- For higher water content the average continuum reflectance level lowers, and the 1–2.6-μm VNIR negative slope becomes steeper.

The band positions almost systematically display a different behavior with temperature, which depends on the absorbing molecule they are related to, provided that evaluable shifts are greater than the spectral resolution. Absorption features corresponding to vibrational modes involving H_2O molecules (especially in natron spectra) typically shift towards longer wavelengths as the temperature decreases. This is explained by an increasing strength of hydrogen bonding as the temperature decreases. Conversely, the absorption bands corresponding to vibrations occurring in CO_3 carbonate ion (bands of natrite) tend to shift towards shorter wavelengths as the temperature decreases, possibly due to phase transition occurring in natrite. An intermediate behavior characterizes the thermonatrite spectrum.
The MAJIS spectro-imager onboard the JUICE mission will closely observe the surface of Jupiter's icy moons with high spectral resolution. In this regard, these laboratory spectra will aid the interpretation of future hyperspectral data in highlighting variations in composition, texture and temperature.

Acknowledgements

The minerals used in this work were obtained as part of the research project: "Key laboratory measurements for Solar System ices" (PI: Dr. Federico Tosi), selected and funded in 2013 by INAF-IAPS in the framework of an internal call for original research projects not otherwise funded. The set of measurements described in this work is the outcome of the research project: "Characterization of Hydrated Na-Carbonates at Cold Planetary Conditions" (PI: Dr. Federico Tosi), selected and funded in 2016 in the framework of the European Union's Horizon 2020 Research Infrastructure (RI) programme (http://www.europlanet-2020-ri.eu), under grant agreement No 654208. This work was partly supported by the Italian Space Agency (ASI) and by the Centre National d'Etude Spatiale (CNES).

References

Anthony J.W., Bideaux R.A., Bladh K.W., and Nichols M.C., 2003. Handbook of Mineralogy. Mineralogical Society of America, Chantilly, VA 20151-1110, USA. http://www.handbookofmineralogy.org/

Arakcheeva A. and Chapuis G., 2005. A reinterpretation of the phase transitions in Na_2CO_3. Acta Crystallographica Section B, 61, 601-607, doi:10.1107/S0108768105033008

Bandfield J.L., Glotch T.D. and Christensen P.R., 2003. Spectroscopic Identification of Carbonate Minerals in the Martian Dust. Science, vol.301, 1084-1087, DOI: 10.1126/science.1088054

Baldridge, A. M., S.J. Hook, C.I. Grove and G. Rivera, 2009. The ASTER Spectral Library Version 2.0. Remote Sensing of Environment, vol. 113, pp. 711-715

Beck, P., Schmitt, B., Cloutis, E.A., Vernazza, P., 2015. Low-temperature reflectance spectra of brucite and the primitive surface of 1-Ceres? Icarus 257, 471–476.

Bonnefoy, N., 2001. Développement d'un spectrophoto-goniomètre pour l'étude de la réflectance bidirectionnelle des surfaces géophysiques. Application au soufre et perspectives pour le satellite Io. Université Joseph Fourier, Grenoble PhD thesis

Boynton W.V., D.W. Ming, S.P. Kounaves, S.M.M. Young, R.E. Arvidson, M.H. Hecht, J. Hoffman, P.B. Niles, D.K. Hamara, R.C. Quinn, P.H. Smith, B. Sutter, D.C. Catling, and R.V. Morris, 2009. Evidence for Calcium Carbonate at the Mars Phoenix Landing Site, Science, 325, 61, pp.61-64, DOI: 10.1126/science.1172768

Brissaud O., Schmitt B., Bonnefoy N., Douté S., Rabou P., Grundy W., and Fily M., 2004. Spectrogonio radiometer for the study of the bidirectional reflectance and polarization functions of planetary surfaces. 1. Design and tests. Applied Optics, vol.43, n.9, pp. 1926-1937

Brooker M.H. and Bates J.B., 1971. Raman and Infrared Spectral Studies of Anhydrous Li_2CO_3 and Na_2CO_3. The Journal of Chemical Physics, vol. 54, N. 11, pp. 4788-4796

Buijs K. and Schutte C.J.H., 1961a. The infrared spectra and structures of Li_2CO_3 and anhydrous Na_2CO_3. Spectrochimica Acta, vol. 17, pp. 927-932

Buijs K. and Schutte C.J.H., 1961b. An infrared study of the hydrates of sodium carbonate. Spectrochimica Acta, vol. 17, pp. 917-920

Carlson R. W., Calvin W. M., Dalton J.B., Hansen G.B., Hudson R.L., Johnson R.E., McCord T.B., Moore M.H., 2009. Europa's Surface Composition, Europa. Edited by Robert T. Pappalardo, William B. McKinnon, Krishan K. Khurana; with the assistance of René Dotson with 85 collaborating authors. University of Arizona Press, Tucson, 2009. The University of Arizona space science series ISBN: 9780816528448, p.283

Carlson, R.W., Weissman, P.R., Smythe, W.D., Mahoney, J.C., 1992. Near-Infrared Mapping Spectrometer experiment on Galileo. Space Sci. Rev. 60 (1–4), p. 457-502. doi: 10.1007/BF00216865.

Carrozzo, F.G., De Sanctis, M.C., Raponi, A., Ammannito, E., Castillo-Rogez, J.C., Ehlmann, B.L., Marchi, S., Stein, N., Ciarniello, M., Tosi, F., Capaccioni, F., Capria, M.T., Fonte, S., Formisano, M., Frigeri, A., Giardino, M., Longobardo, A., Magni, G., Palomba, E., Zambon, F., Raymond, C.A., Russell, C.T., 2018. Nature, formation and distribution of carbonates on Ceres. Sci. Adv. 4 (3), e1701645. doi:10.1126/sciadv.1701645.

Catling D.C., 1999. A chemical model for evaporites on early Mars: Possible sedimentary tracers of the early climate and implications for exploration. Journal of Geophysical Research, vol.104, E7, pp. 16,453-16,469

Clark, R.N., Roush, T.L., 1984. Reflectance Spectroscopy: quantitative analysis techniques for remote sensing applications. Journal of Geophysical Research 89 (B7), 6329–6340

Clark, R.N., King, T.V.V., Klejwa, M., Swayze, G., 1990. High spectral resolution reflectance spectroscopy of minerals. Journal of Geophysical Research 95 (B8), 12653–12680

Crowley J. K., 1991. Visible and near-infrared (0.4-2.5 μm) reflectance spectra of playa evaporate minerals. Journal of Geophysical Research, 96, pp.16,231-16,240

Dalton J.B., Prieto-Ballesteros O., Kargel J.S., Jamieson C.S., Jolivet J., Quinn R., 2005. Spectral comparison of heavily hydrated salts with disrupted terrains on Europa. Icarus 177, 472–490

De Angelis S., Carli C., Tosi F., Beck P., Schmitt B., Piccioni G., De Sanctis M.C., Capaccioni F., Di Iorio T., Philippe S., 2017. Temperature-dependent VNIR spectroscopy of hydrated Mg-sulfates. Icarus 281, 444–458

De Sanctis, M.C., Coradini, A., Ammannito, E., Filacchione, G., Capria, M.T., Fonte, S., Magni, G., Barbis, A., Bini, A., Dami, M., Ficai-Veltroni, I., Preti, G. and the VIR Team, 2011. The VIR spectrometer. Space Sci. Rev. 163 (1–4), 329–369. doi:10. 1007/s11214- 010- 9668- 5.

De Sanctis M.C., Raponi A., Ammannito E., Ciarniello M., Toplis M.J., McSween H.Y., Castillo-Rogez J.C., Ehlmann B.L., Carrozzo F.G., Marchi S., Tosi F., Zambon F., Capaccioni F., Capria M.T., Fonte S., Formisano M., Frigeri A., Giardino M., Longobardo A., Magni G., Palomba E., McFadden L.A., Pieters C.M., Jaumann R., Schenk P., Mugnuolo R., Raymond C.A. & Russell C.T., 2016. Bright carbonate deposits as evidence of aqueous alteration on (1) Ceres, Nature Letter, vol.536, p.54-57, doi:10.1038/nature18290

De Sanctis, M.C., Ammannito, E., McSween, H.Y., Raponi, A., Marchi, S., Capaccioni, F., Capria, M.T., Carrozzo, F.G., Ciarniello, M., Fonte, S., Formisano, M., Frigeri, A., Giardino, M., Longobardo, A., Magni, G., McFadden, L.A., Palomba, E., Pieters, C.M., Tosi, F., Zambon, F., Raymond, C.A., Russell, C.T., 2017. Localized aliphatic organic material on the surface of Ceres. Science 355 (6326), 719–722. doi:10.1126/science.aaj2305.

Drake N., 1995. Reflectance spectra of evaporite minerals (400-2500 nm): Applications for remote sensing. Int. J. Remote Sens. 16, 2555-2571. http://dx-doi.org/10.1080/01431169508954576

Ehlmann B.L., Mustard J.F., Murchie S.L., Poulet F., Bishop J.L., Brown A.J., Calvin W.M., Clark R.N., Des Marais D.J., Milliken R.E., Roach L.H., Roush T.L., Swayze G.A., Wray J.J., 2018. Orbital Identification of Carbonate-Bearing Rocks on Mars. Science, 322, pp.1828-1832

Ehlmann B.L. and Edwards C.S., 2014. Mineralogy of the Martian Surface. Annual Review Earth and Planetary Science, 42, pp.291–315

Farmer, V. C., 1974. The vibrations of protons in minerals: hydroxyl, water, and ammonium, in The infrared spectra of minerals, edited by V. C. Farmer, pp. 137-181, Mineralogical Society, London

Gaffey S.J., 1986. Spectral reflectance of carbonate minerals in the visible and near infrared (0.35-2.55 microns): calcite, aragonite, and dolomite. American Mineralogist, Volume71, pages 151-162

1101 Grisolle, F., 2013. Les condensats saisonniers de Mars : étude expérimentale de la formation et
1102 du métamorphisme de glaces de CO_2. Université Joseph Fourier, Grenoble PhD thesis.
1103
1104 Grisolle, F., Schmitt, B., Beck, P., Philippe, S., Brissaud, O., 2014. Experimental simulation of the
1105 condensation and metamorphism of seasonal CO_2 condensates under martian conditions.
1106 European Planetary Science Congress, EPSC Abstracts, 9 EPSC2014-635-1.
1107
1108 Grotzinger, J. and R. Milliken (eds.) 2012. Sedimentary Geology of Mars. SEPM
1109
1110 Grundy W.M. and Schmitt B., 1998. The temperature-dependent near-infrared absorption
1111 spectrum of hexagonal H_2O ice. Journal of Geophysical Research, vol. 103, N. E11, pp. 25,809-
1112 25,822
1113
1114 Gundlach B. and Blum J.: A new method to determine the grain size of planetary regolith,
1115 Icarus 223, pp. 479-492, 2013
1116
1117 Hapke, B., 1993. Theory of Reflectance and Emittance Spectroscopy. Cambridge University
1118 Press, p. 455. http://dx.doi.org/10.1017/CBO9780511524998. Online ISBN 9780511524998
1119
1120 Harloff J. and Arnold G., 2001. Near-infrared reflectance spectroscopy of bulk analog materials
1121 for planetary crust. Planetary and Space Science 49, 191–211
1122
1123 Harner P.L. and Gilmore M.S., 2014. Are Martian Carbonates Hiding In Plain Sight? Vnir
1124 Spectra Of Hydrous Carbonates. 45th Lunar and Planetary Science Conference, abstract
1125 n.2728
1126
1127 Harner P.L. and Gilmore M.S., 2015. Visible–near infrared spectra of hydrous carbonates, with
1128 implications for the detection of carbonates in hyperspectral data of Mars. Icarus 250, 204–
1129 214
1130
1131 Harris M.J. and Salje E.K.H., 1992. The incommensurate phase of sodium carbonate: an
1132 infrared absorption study. Journal of Physics, Condensed Matter, 4, pp. 4399-4408
1133
1134 Hunt, G.R. & Salisbury, J.W., 1971. Visible and near infrared spectra of minerals and rocks. II.
1135 Carbonates. Mod. Geol. 2, 23–30
1136
1137 Jones A.P., Genge M., Carmody L., 2013: Carbonate Melts and Carbonatites. Reviews in
1138 Mineralogy & Geochemistry, Vol. 75, pp. 289-322
1139
1140 Jones, B.F., Deocampo, D.M., 2003. Geochemistry of Saline Lakes, cap.5.13. In: Holland,
1141 Heinrich, Turekian, Karl (Eds.), Treatise on Geochemistry Editors-in-Chief. Published by
1142 Elsevier, ISBN: 978-0-08-043751-4 doi: 10.1016/ B978- 0- 08- 095975- 7.09816- 8
1143
1144 Khomyakov A.P., 1983. Natrite, Na_2CO_3 – a new mineral. International Geology Review Vol. 25,
1145 Iss. 9
1146
1147 McCord T.B., Hansen G.B., Fanale F.P., Carlson R.W., Matson D.L., Johnson T.V., Smythe W.D.,
1148 Crowley J.K., Martin P.D., Ocampo A., Hibbitts C.A., Granahan J.C., and the Galileo NIMS team.
1149 1998a. Salts On Europa's Surface From The Galileo Nims Investigation. Lunar and Planetary
1150 Science Conference XXIX, LSPC abstract N.1560

McCord T.B., Hansen G.B., Fanale F.P., Carlson R.W., Matson D.L., Johnson T.V., Smythe W.D., Crowley J.K., Martin P.D., Ocampo A., Hibbitts C.A., Granahan J.C., and the Galileo NIMS team. 1998b. Salts on Europa's Surface Detected by Galileo's Near Infrared Mapping Spectrometer. Science, 280, pp. 1242-1245, DOI: 10.1126/science.280.5367.1242

McCord T.B., Hansen G.B., Matson D.L., Johnson T.V., Crowley J.K., Fanale F.P., Carlson R.W., Smythe W.D., Martin P.D., Hibbitts C.A., Granahan J.C., and Ocampo A., 1999. Hydrated salt minerals on Europa's Surface from the Galileo near-infrared mapping spectrometer (NIMS) investigation. Journal of Geophysical Research, vol. 104, No. E5, pages 11,827-11,851

McCord T.B., Orlando T.M., Teeter G., Hansen G.B., Sieger M.T., Petrik N.G. and Van Keulen L., 2001. Thermal and radiation stability of the hydrated salt minerals epsomite,mirabilite, and natron under Europa environmental conditions. Journal of Geophysical Research, vol. 106, No. E2, pages 3311-3319

McCord T.B., Hansen G.B., Combe J.-P., Hayne P., 2010. Hydrated minerals on Europa's surface: An improved look from the Galileo NIMS investigation. Icarus, 209, 639–650

McLennan S.M., 2012. Geochemistry of Sedimentary Processes on Mars. Book Chapter, in Sedimentary Geology of Mars, Society for Sedimentary Geology, special publication, vol.102, ISBN electronic: 9781565763135, GeoScienceWorld, in https://doi.org/10.2110/pec.12.102.0119

Meekes H., Rasing Th., and Wyder P., 1986. Raman and infrared spectra of the incommensurate crystal Na_2CO_3. Physical Review B, vol. 34, N. 6, pp.4240-4254

Morris R.W., Ruff S.W., Gellert R., Ming D.W., Arvidson R.E., Clark B.C., Golden D.C., Siebach K., Klingelhöfer G., Schröder C., Fleischer I., Yen A.S., Squyres S.W., 2010. Identification of Carbonate-Rich Outcrops on Mars by the Spirit Rover, Science, 329, pp.421-424

Niles P.B., Catling D.C., Berger G., Chassefière E., Ehlmann B.L., Michalski J.R., Morris R., Ruff S.W., Sutter B., 2013. Geochemistry of Carbonates on Mars: Implications for Climate History and Nature of Aqueous Environments. Space Science Review 174, 301–328 DOI 10.1007/s11214-012-9940-y

Nuevo M., Sandford S.A., Flynn G.J., And Wirick S., 2014. Mid-infrared study of stones from the Sutter's Mill meteorite. Meteoritics & Planetary Science 49, Nr 11, 2017–2026, doi: 10.1111/maps.12269

Piccioni, G., Langevin, Y., Filacchione, G., Poulet, F., Tosi, F., Eng, P., Dumesnil, C., Zambelli, M., Saggin, B., Fonti, S., Grassi, D., Altieri, F., 2014. MAJIS, the Moons And Jupiter Imaging Spectrometer, designed for the future ESA/JUICE mission. Geophys. Res. Abstr. 16 EGU2014-10925-2, EGU General Assembly.

Postberg F., Kempf S., Schmidt J., Brilliantov N., Beinsen A., Abel B., Buck U. and Srama R., 2009. Sodium salts in E-ring ice grains from an ocean below the surface of Enceladus. Nature Letters, vol.459, pp.1098-1101, doi:10.1038/nature/08046

Postberg F., Schmidt J., Hillier J., Kempf S. and Srama R., 2011. A salt-water reservoir as the source of a compositionally stratified plume on Enceladus. Nature Letters, vol.474, pp. 620-622, doi:10.1038/nature10175

Raponi A., De Sanctis M.C., Carrozzo F.G., Ciarniello M., Castillo-Rogez J.C., Ammannito E., Frigeri A., Longobardo A., Palomba E., Tosi F., Zambon F., Raymond C.A., Russell C.T., 2018. Mineralogy of Occator crater on Ceres and insight into its evolution from the properties of carbonates, phyllosilicates, and chlorides. Icarus, 2018, in press, https://doi.org/10.1016/j.icarus.2018.02.001

Russo, M., 2006. I minerali di formazione fumarolica della grande eruzione vesuviana del 1906. http://www.ov.ingv.it/ov/doc/ofr06006.pdf, 2006

Tosi F., De Sanctis M.C., Krohn K., Zambon F., Ammannito E., Capria M.T., Carrozzo F.G., Ciarniello M., Combe J.-Ph., Formisano M., Frigeri A., Jaumann R., Longobardo A., Palomba E., Raponi A., Raymond C.A., Russell C.T., Schorghofer N., 2016. Thermal Behavior Of Bright Spots On Ceres, 47th Lunar and Planetary Science Conference, LPSC, abstract n.1883

Vu T.H., Hodyss R., Johnson P.V., Choukroun M., 2017. Preferential formation of sodium salts from frozen sodium-ammonium-chloride-carbonate brines – Implications for Ceres' bright spots. Planetary and Space Science, 141, 73–77

Wray J.J., Murchie S.L., Bishop J.L., Ehlmann B.L., Milliken R.E., Wilhelm M.B., Seelos K.D., and Chojnacki M., 2016. Orbital evidence for more widespread carbonate-bearing rocks on Mars. Journal of Geophysical Research Planets, 121, 652–677, doi:10.1002/2015JE004972

Zolotov M.Y., 2017. Aqueous origins of bright salt deposits on Ceres. Icarus, 296, 289–304